The oxidative stress response, in particular the *katY* gene, is temperature-regulated in *Yersinia pseudotuberculosis*

Daniel Scheller[1], Franziska Becker[1], Andrea Wimbert[1], Dominik Meggers[1], Stephan Pienkoß[1], Christian Twittenhoff[1], Lisa R. Knoke[2], Lars I. Leichert[2], Franz Narberhaus[1*]

[1]Ruhr University Bochum, Faculty of Biology and Biotechnology, Microbial Biology, 44780 Bochum, Germany

[2]Ruhr University Bochum, Faculty of Medicine, Institute of Biochemistry and Pathobiochemistry, Microbial Biochemistry, 44780 Bochum, Germany

Short title: *Yersinia* oxidative stress response regulation

*** Corresponding author:** franz.narberhaus@rub.de

Abstract

Pathogenic bacteria, such as *Yersinia pseudotuberculosis* encounter reactive oxygen species (ROS) as one of the first lines of defense in the mammalian host. In return, the bacteria react by mounting an oxidative stress response. Previous global RNA structure probing studies provided evidence for temperature-modulated RNA structures in the 5'-untranslated region (5'-UTR) of various oxidative stress response transcripts, suggesting that opening of these RNA thermometer (RNAT) structures at host-body temperature relieves translational repression. Here, we systematically analyzed the transcriptional and translational regulation of ROS defense genes by RNA-sequencing, qRT-PCR, translational reporter gene fusions, enzymatic RNA structure probing and toeprinting assays. Transcription of four ROS defense genes was upregulated at 37°C. The *trxA* gene is transcribed into two mRNA isoforms, of which the short one contains a functional RNAT. Biochemical assays validated temperature-responsive RNAT-like structures in the 5'-UTRs of *sodB*, *sodC* and *katA*. However, they barely conferred translational repression in *Y. pseudotuberculosis* at 25°C suggesting partially open structures available to the ribosome in the living cell. Upstream of *katY* we uncovered a novel, highly efficient RNAT that was primarily responsible for massive induction of KatY at 37°C. By phenotypic characterization of catalase mutants and through fluorometric real-time measurements of the redox-sensitive roGFP2-Orp1 reporter in these strains, we revealed KatA as the primary H_2O_2 scavenger. Consistent with temperature regulation of *katY*, we observed an improved protection of *Y. pseudotuberculosis* at 37°C. Our findings suggest a multilayered regulation of the oxidative stress response in *Yersinia* and an important role of RNAT-controlled *katY* expression at host body temperature.

Author summary

The external conditions dramatically change when a bacterial pathogen enters a mammalian host. Sensing the new situation and rapidly responding to it is of critical importance for pathogens, like *Yersinia pseudotuberculosis*, since they often circulate between their environmental reservoirs and a warm-blooded host. Many virulence-related genes encode a temperature-sensitive mRNA element, a so-called RNA thermometer (RNAT), in the 5'-end of their transcript. Melting of this structure at 37°C allows ribosome binding and translation initiation. The host immune system typically fights microbial pathogens by the production of reactive oxygen species (ROS). Here, we find that several ROS defense genes in *Yersinia* are upregulated at host body temperature to counteract the ROS attack. In particular, the massive RNAT-mediated upregulation of the catalase KatY confers protection against H_2O_2 at 37°C. Our study reveals a close regulatory link between temperature sensing and the oxidative stress response in a notorious food borne pathogen.

1 Introduction

All bacteria encounter oxidative stress caused by reactive oxygen species (ROS), such as superoxide (O_2^-), hydrogen peroxide (H_2O_2) and hydroxyl radicals [1]. ROS either accumulate endogenously by processes like aerobic metabolism and iron-sulfur cluster oxidation [2] or by exogenous exposure through their environment. Environmental H_2O_2 concentrations can rise due to excretion of H_2O_2 by lactic acid bacteria or as a response of the host immune response [3]. These sources of exogenous ROS are especially relevant for pathogenic bacteria, causing intestinal infections during gut colonization [4]. One such bacterium is the food borne pathogen

66 *Yersinia pseudotuberculosis*, which leads to gastrointestinal diseases, like acute
67 abdominal pain, mesenteric lymphadenitis or diarrhea [5].

68 To overcome oxidative stress induced challenges, bacteria have developed multiple
69 strategies to combat ROS. O_2^- can be transformed by superoxide dismutases into O_2
70 and H_2O_2, which can be further neutralized by catalases into H_2O and O_2. Furthermore,
71 H_2O_2 is scavenged by alkyl hydroperoxide reductases [3]. ROS often oxidize a variety
72 of proteins containing cysteine residues. This results in non-native disulfide bond
73 formation, which often causes a loss of function. Antioxidants, such as thioredoxins
74 and glutathione-dependent glutaredoxins reduce these disulfide bonds in the
75 cytoplasm and restore protein function [6].

76 A temperature upshift is one of the first and most reliable cues for pathogens signaling
77 the entry into a warm-blooded host from a comparatively cool environment.
78 Accordingly, many pathogenic bacteria induce the expression of virulence genes at
79 37°C [7–9]. This also applies to *Y. pseudotuberculosis* and its close relative *Yersinia*
80 *pestis*. LcrF, the master regulator of virulence, is induced at 37°C by multiple means.
81 At ambient temperatures, transcription of *lcrF* is repressed by the nucleoid-associated
82 protein YmoA. Upon a temperature upshift, YmoA is degraded by the ClpP and Lon
83 proteases, relieving transcriptional repression [10]. In addition, translation of the *lcrF*
84 mRNA is blocked by an RNA thermometer (RNAT), which sequesters the ribosome
85 binding site (RBS) at low temperatures and thereby prevents access of the ribosome.
86 At 37°C this RNAT melts and releases the RBS, allowing LcrF synthesis [11]. LcrF
87 acts as a transcriptional activator for several virulence-associated genes located on
88 the virulence plasmid pYV, which code for the type III secretion system (T3SS),
89 effector proteins translocated by the T3SS, or the adhesin YadA [12].

Strikingly, these typical virulence genes are far from being the only ones affected by temperatures changes. RNA sequencing revealed more than 300 differentially transcribed genes between 25 and 37°C [13]. Among them are genes of the oxidative stress response, namely the genes coding for the superoxide dismutases SodB and SodC and the catalases KatA and KatY (Fig. 1). Apart from this transcriptional regulation, global RNA structuromics approaches revealed the existence of RNATs upstream of numerous genes suggesting a contribution to sensing and responding to a warm-blooded host [14,15]. Several of the RNAT-regulated genes play a direct role in virulence, such as the genes for the adhesion protein AilA [14], the virulence factor OmpA [16], the T3SS components YscJ and YscT [17], the T3SS regulator YopN [18], and the secreted bacterial toxin CnfY [19].

As in many other bacteria, the transcriptional regulator OxyR is the master regulator of H_2O_2 defense genes in *Yersinia* species [20,21]. The striking existence of putative RNATs upstream of several oxidative stress response genes, more specifically *sodB, sodC, katA, katY* and *trxA* [14,15] (Fig. 1), however, suggested an additional temperature-responsive regulation of ROS defense genes in *Y. pseudotuberculosis*. In support of a role of catalases in the warm-blooded host, previous reports in *Y. pestis* showed that KatY is a temperature-regulated protein [22,23]. The underlying mechanism of preferential *katY* expression at 37°C remained elusive, but a predicted secondary structure in the 5'-untranslated region (5'-UTR) was taken as evidence for an RNAT-like mechanism [21].

In this study, we investigated transcriptional and translational control mechanisms of various ROS defense genes in *Y. pseudotuberculosis*. We used a broad range of *in vitro* and *in vivo* approaches to tease apart the different control levels. This work

provides detailed insights into the regulation of five ROS detoxification genes. We paid particular attention to the biological roles of the catalases KatA and KatY and identified a novel RNAT upstream of *katY*. Physiologically, KatY confers improved protection against H_2O_2 at 37°C.

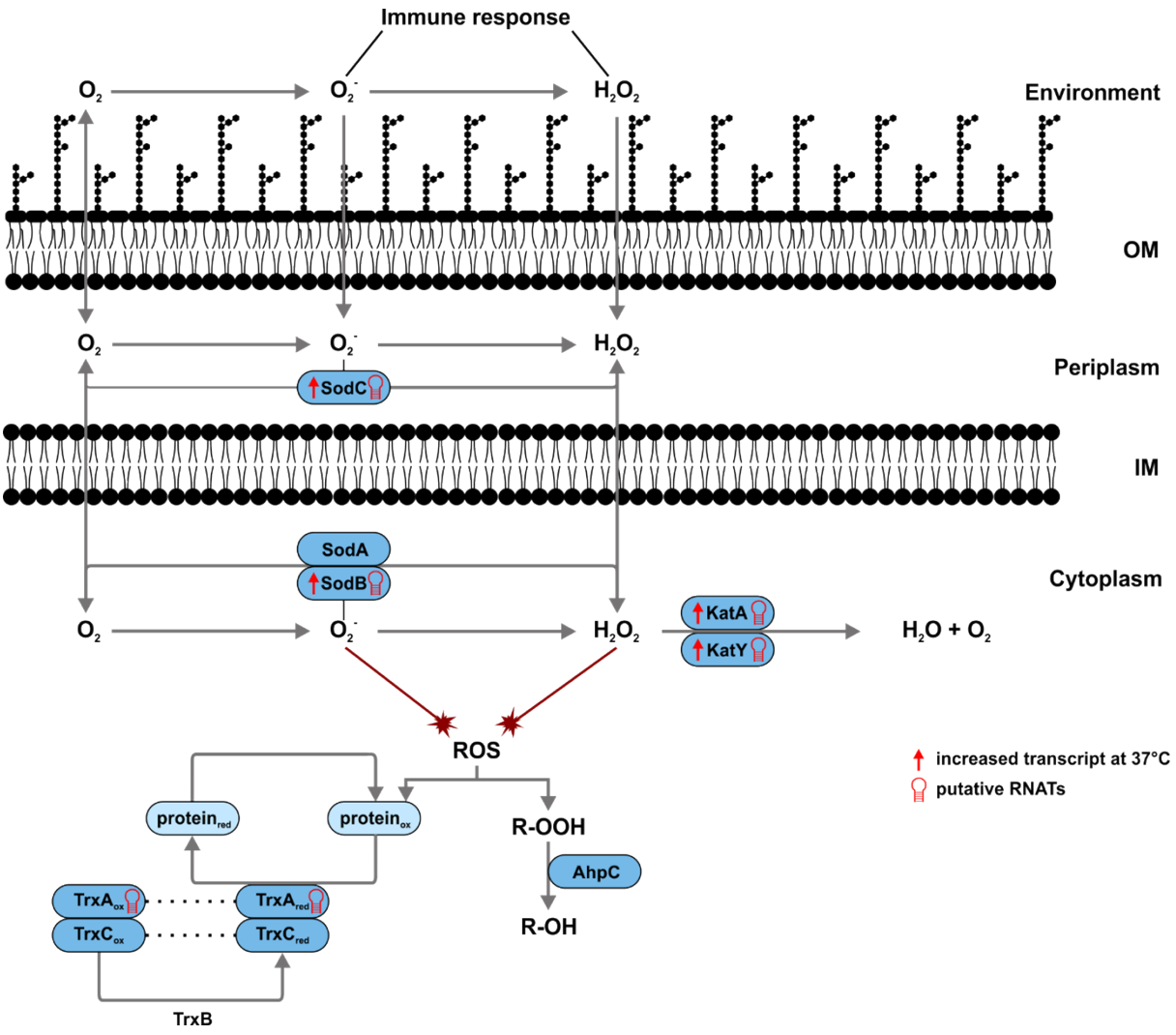

Figure 1. ROS detoxification pathways in *Y. pseudotuberculosis* and potential temperature regulation mechanisms. Superoxide and hydrogen peroxide are released by the immune response of the host and enter the bacterial cell. The periplasmic superoxide dismutase SodC encounters superoxide first and, together with its cytoplasmic equals SodA and SodB, transforms it into hydrogen peroxide. This is further neutralised by the catalases KatA and KatY into water and oxygen. Proteins, which have been oxidized by ROS, can be reduced by the thioredoxins TrxA and TrxC. TrxB is responsible for returning the thioredoxins to their reduced state. The alkyl hydroperoxide reductase AhpC is furthermore involved in the detoxification of hydrogen peroxide and its derivatives by converting them to water and alcohols. It is the primary scavenger of endogenously generated hydrogen peroxides. Increased transcription [13] or putative translation [14,15] at 37 compared to 25°C of ROS detoxification genes is indicated.

2 Material and Methods

2.1 Bacterial strains and plasmids

Bacterial strains used in this study are listed in table S2. Cells were grown in lysogeny broth (LB; 1 % NaCl, 1 % Tryptone and 0.5 % yeast extract) at indicated temperatures. Cultures were supplemented with 150 µg/ml ampicillin or 30 µg/ml chloramphenicol when necessary.

2.2 Plasmid construction

All used plasmids and oligonucleotides are listed in tables S3 and S4, respectively. Point mutations were generated by site-directed mutagenesis according to the instruction manual of the QuikChange® mutagenesis kit (Agilent Technologies).

The RNAT-*bgaB* fusion plasmids (pBO4909 and pBO4436) were constructed by amplifying the 5'-UTR including 30 bp of the coding region with the respective primers sodC_UTR_fw/sodC_UTR_rev and katY_UTR_fw/katY_UTR_rev, digested with NheI and EcoRI and ligated into pBAD2-*bgaB*-His. To introduce mutations into the RNAT-*bgaB* plasmids their respective rep or derep primers were used with the RNAT-*bgaB* plasmids as a template.

The run-off plasmid for *in vitro* transcription of the RNATs were generated by blunt-end ligation of a PCR-amplified DNA fragment (respective primers RNAT_ro_fw/RNAT_ro_rev), containing the T7 promoter, the RNAT and 60 bp of the coding region, into the EcoRV or NaeI restriction site of pUC18. To introduce mutations into the RNAT-runoff plasmids their respective rep or derep primers were used with the RNAT-runoff plasmids as template.

For deletion of the *katA* and *katY* gene, two fragments flanking the target gene, with

an overlap to each other, were constructed by PCR with primers katA/Y 5'flank_fw/rev and katA/Y 3'flank_fw/rev and recombined by SOE-PCR [24]. This fragment was cloned into the pDM4-suicide plasmid after restriction with SalI and XbaI and transferred to *Y. pseudotuberculosis* by conjugation with *E. coli* S17-1 λ-pir. After selection on LB plates with 10 % sucrose, chloramphenicol-sensitive and sucrose-resistant colonies were checked for deletion of the target gene using the katA/Y_EP_fw/rev and katA/Y_IP_fw/rev primer pairs and verified by DNA sequencing (pBO6868; Δ*katA* and pBO7212; Δ*katY*).

For complementation of the deletion strains, NEBuilder HiFi DNA Assembly was utilized. The plasmids pBO6868 and pBO7212 were linearized by PCR amplification using the primer pairs pDM4_katA/Y_Del_fw and pDM4_katA/Y_Del_rev, respectively.

The 5'-UTR with the coding region of *katA* or *katY* and a C-terminal His-Tag were amplified using the primer pairs katA/Y-His_fw and katA/Y-His_rev. In a second amplification, an overlap to the linearized pBO6868 and pBO7212 plasmids was added using the primers katA/Y_pDM4_Del_fw and katA/Y_pDM4_Del_rev. The linearized plasmid and the complementation fragment with the overlap were mixed and assembled, using the NEBuilder HiFi DNA Assembly according to manufacturer's instructions. After successful assembly, the plasmid was transferred into *Y. pseudotuberculosis* by conjugation and after double homologous recombination, colonies were checked for complementation of the target gene using the same primers as for the deletion strains and verified by DNA sequencing (pBO6888; Δ*katA* + *katA*-His ; pBO7251; Δ*katY* + *katY*-His). Additionally, the same procedure was used to generate the complementation plasmid pBO7246. Linearization of the pBAD-His A plasmid was achieved by use of the primers pBAD-His_fw/rev and the overlap for the

179 *katY*-His fragment was amplified using primers katY_pBAD_fw and His_pBAD_rev.

180 **2.3 Reporter gene activity assay**

181 *E. coli* DH5α or *Y. pseudotuberculosis* YPIII cells carrying the various RNAT-*bgaB*
182 fusion plasmids were inoculated to an optical density at 600 nm (OD_{600}) of 0.1. After
183 growth to an OD_{600} of 0.5 at 25°C, transcription was induced with 0.01 % in *E. coli* or
184 0.1 % in *Y. pseudotuberculosis*, L-arabinose. The culture was split and shifted to 25
185 and 37°C. After incubation for 30 min, 400 µl samples were subsequently taken for β-
186 galactosidase assay, 2 ml samples for Western blotting and 4 ml samples for RNA
187 isolation. The β-galactosidase assay was carried out as described previously [25].

188 **2.4 Western blot analysis**

189 Cell pellets were resuspended according to their optical density (100 µl per OD_{600} of 1)
190 in 1 x SDS sample buffer (2 % SDS, 0.1 % bromophenol blue, 1 % 2-mercaptoethanol,
191 25 % glycerol, 50 mM Tris/HCl, pH 6.8). After centrifugation (10 min, 13000 rpm),
192 samples were boiled for 10 min at 95°C, and the supernatant was loaded and
193 separated by SDS gel electrophoresis in 5 % stacking and 12 % separating gels. By
194 tank blotting, the proteins were transferred onto a nitrocellulose membrane (Hybond-
195 C Extra, GE Healthcare) and an anti-His-HRP conjugate antibody (Bio-Rad) was used
196 in a 1:4000 dilution. Chemiluminescence signals were detected by incubating
197 membranes with Immobilon Forte Western HRP substrate (Millipore) with a ChemiDoc
198 MP Imaging System (Biorad).

199 **2.5 Quantitative Western blot analysis**

200 Samples were prepared as described above. The supernatant was separated by SDS
201 gel electrophoresis in TGX Stain-Free FastCast 12 % Acrylamide Gels (Biorad). After
202 separation, the Stain-Free visualization was enabled by activation of the gels for 45

seconds with UV-light before the proteins were transferred by Trans-Blot Turbo Transfer (Biorad) onto a nitrocellulose membrane (Trans-Blot Turbo RTA, Biorad). A mouse anti-His antibody (Biorad) was used as a primary antibody in a 1:500 dilution. A goat anti-mouse IgG StarBright Blue 700 fluorescent antibody (Biorad) was used as a secondary antibody in a 1:2500 dilution. Fluorescence signals and Stain-Free Imaging were detected in a ChemiDoc MP Imaging System (Biorad). The fluorescence signals were quantified by normalization to the total protein amount detected by Stain-Free visualization, after determining the linear range using Image Lab (Biorad).

2.6 RNA extraction and quantitative reverse transcription PCR (qRT-PCR)

Using the peqGOLD Trifast reagent according to the manufacturer's protocol, total RNA was extracted. RNA samples were treated with Turbo™ DNase (TURBO DNA-free™ Kit, Invitrogen) to remove DNA contamination. Synthesis of cDNA was performed using the iScript™ cDNA synthesis Kit (Bio-Rad) according to the manufacturer's protocol with 1 µg RNA per reaction. 2 µl of 1:10 diluted cDNA were mixed with 250 nM of each primer, 5 µl of 2x iTaq Universal SYBR Green Supermix, and 2.5 µl sterile water (Carl Roth). In a CFX Connect™ Real-Time System (Bio-Rad) the amplification and detection of PCR products was measured. To calculate primer efficiency and determine the linear range of amplification, standard curves were employed. Relative transcript amounts were calculated using the primer efficiency corrected method [26]. The non-thermoregulated reference genes *gyrB* and *nuoB* were used for normalization.

2.7 In vitro transcription

RNA for structure probing and primer extension inhibition experiments were synthesized *in vitro* by run-off transcription with T7 RNA polymerase (Thermo

Scientific) from EcoRV- or NaeI-linearized pUC18-RNAT + 60 nt plasmids (listed in table S3) as previously described [14].

2.8 Enzymatic RNA structure probing

RNA structure probing of the 5'-UTR and 60 nt of the RNATs was performed with *in vitro* transcribed RNA. 5'-[^{32}P]-labeled RNA (30000 cpm) was mixed with buffer and tRNAs, preincubated for 5 min at various temperatures and treated with T1 (0.0017U) (Invitrogen) or T2 (0.075U) (MoBiTec) RNases for 5 min. For digestion, 5x TN buffer (100 mM Tris acetate, pH 7, 500 mM NaCl) was used. An alkaline hydrolysis ladder and T1 ladder were prepared as described in [27]. All reactions were stopped by addition of formamide loading dye and boiling at 95°C. Samples were separated on an 8-12 % denaturing polyacrylamide gel.

2.9 Primer extension inhibition analysis (toeprinting)

Toeprinting analysis was performed with 30S ribosomal subunits, *in vitro* transcribed RNA and tRNA^{fMet} (Sigma-Aldrich) according to [28]. The 5'-[^{32}P]-labeled oligonucleotide "gene"_ro_rv, complementary to the 3'end of the *in vitro* transcribed RNA of interest, was used as a primer for cDNA synthesis. The radiolabeled primer (0.16 pmol) was annealed to the RNAT-mRNA (0.08 pmol), incubated with 30S ribosomal subunits (12 pmol) or Tico buffer (60 mM HEPES/KOH, 10.5 mM $Mg(CH_3COO)_2$, 690 mM NH_4COO, 12 mM 2-mercaptoethanol, 10 mM spermidine, 0.25 mM spermine) in presence of tRNA^{fMet} (8 pmol) at 25°C, 37°C or 42°C for 10 min. Synthesis of cDNA was performed for 10 min at 37°C after addition of 2 µl MMLV-Mix (VD+Mg^{2+} buffer, BSA, dNTPs and 800 U MMLV reverse transcriptase (Invitrogen). The Reaction was stopped by addition of formamide loading dye and boiling at 95°C. Samples were separated on an 8-12 % denaturing polyacrylamide gel. The Thermo

Sequenase cycle sequencing Kit (Applied Biosystems) was used for sequencing reactions with the pUC18-RNAT+ 60 bp plasmids as template and radiolabeled primer "gene"_ro_rv.

2.10 Zone of inhibition assay

Overnight cultures of various *Y. pseudotuberculosis* strains, grown at 25 and 37°C were diluted to an optical density at 600 nm (OD_{600}) of 0.1. A total of 100 µl was added to 5 ml of softagar, briefly mixed and poured on 15 ml LB plates. A Whatman paper disk was applied to the center of the plate and loaded with 3 µl of 5.5 M H_2O_2. After incubation for 24 h at 25 and 37°C, the zone of inhibition was measured.

2.11 Growth under various H_2O_2 concentrations

Cells of the early exponential phase grown at 25 and 37°C were diluted to an optical density at 600 nm (OD_{600}) of 0.05 and 100 µl were transferred into a clear 96-well plate. 1 µl of various H_2O_2 concentrations were added to the wells to the indicated concentration. Growth was recorded over 20 h at 25 and 37°C.

2.12 Measurement of roGFP2-based probe oxidation state

Oxidation of roGFP2-Orp1 was measured as described in [29] and normalized according to [30] for OxD calculation with slight variation in the experimental setup. Briefly, *Y. pseudotuberculosis* cells of various strains harboring the roGFP2 plasmids were inoculated to an optical density at 600 nm (OD_{600}) of 0.1 and grown at 25 and 37°C. After growth to an OD_{600} of 0.5, expression was induced with 100 µM IPTG and incubated overnight at 25 or 37°C. Cells were washed twice in PBS and resuspended in PBS to an OD_{600} of 0.2 before 100 µl were transfered into a black, clear-bottom 96-well plate (Nunc, Thermo Scientific). Fluorescence intensities were recorded over 10 min in a microplate reader (Infinite M Plex, Tecan) at the excitation wavelengths 405

and 488 nm and emission wavelength of 530 nm at room temperature. Afterwards, 1 µl of 100 mM AT-2 (2,2′-Dipyridyl disulfide), 1 M DTT (Dithiothreitol) or H_2O_2 to the indicated concentrations were added. Changes in fluorescence intensities were measured for 2 h.

2.13 Catalase activity assay

For determining catalase activity, decomposition of H_2O_2 was measured over time by UV-light according to [31]. Early-exponential cells were harvested after growth at 25 or 37°C, resuspended in phosphate buffer (degassed 17 mM sodium phosphate buffer, pH 8.3) and lysed by ultrasonication. Cell debris were removed by centrifugation for 20 min at 21.000 g and 4°C. After Bradford determination, 50 µg of supernatant proteins were mixed with phosphate buffer to a volume of 180 µl. The absorption at 240 nm was monitored for 1 min at 25°C in a quartz cuvette before adding 20 µl of 0.1 M hydrogen peroxide. As a blank, phosphate buffer mixed with H_2O_2 was used. After addition, the absorption of H_2O_2 was continuously monitored, until the reaction left the linear range. The velocity of H_2O_2 decomposition was calculated based on the linear range.

3 Results

3.1 Elevated transcription of several oxidative stress response genes at 37°C

A previously conducted transcriptome study revealed that multiple oxidative stress response genes are upregulated at 37°C compared to 25°C [13]. We compared these findings with previously obtained RNA-seq data from our group (Table S1) and validated the transcription of selected genes by qRT-PCR. Consistent with the published results, some but not all genes involved in ROS detoxification showed an upregulation at 37°C (Fig. 2). Apart from the transcripts encoding the superoxide dismutases SodB and SodC and the catalase KatA, the *katY* mRNA stood out with an about 30-fold induction in all three experiments.

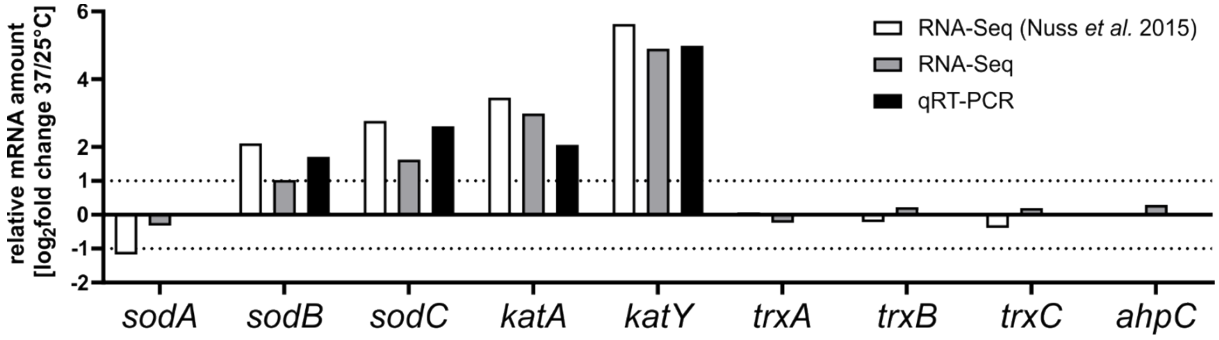

Figure 2. Transcription of four ROS detoxification genes is elevated at 37°C. Relative transcript levels (37/25°C) are shown. White and grey columns represent RNA-Seq data from [13] and this study, respectively. Black columns represent qRT-PCR results of selected targets. RNA was isolated from exponentially grown *Y. pseudotuberculosis* cells at 25 and 37°C. For qRT-PCR, the obtained data were normalized to *gyrB* and *nuoB* as reference genes.

3.2 The 5'-UTRs of oxidative stress response genes contain putative RNATs

Various transcriptional and post-transcriptional mechanisms can account for the upregulation of ROS defense genes under virulence conditions. Previous global structure probing approaches suggested at least some contribution of translational

314 control by temperature-modulated RNATs [14,15]. To validate and extend these
315 findings, we translationally fused candidate 5'-UTRs to *bgaB* encoding a heat-stable
316 and His-tagged beta-galactosidase and measured its activity and protein amount at
317 25 and 37°C (Fig. 3A). This reporter gene system uncouples the native transcription
318 from translation since transcription is controlled by the arabinose-inducible pBAD
319 promoter. The recently described *yopN* RNAT [18] served as positive control. The
320 *sodA* gene, which does not contain an obvious RNAT in its 5'-UTR and is barely
321 temperature-regulated at the translational level [14] was chosen as negative control.

322 First, we investigated the putative RNATs for their ability to control translation in *E. coli*
323 as a host (Fig. 3B). For the catalase genes *katA* and *katY*, we observed a pronounced
324 increase in beta-galactosidase activity and protein amount at 37°C. This was much
325 less evident for the *sod* genes, in particular *sodA* (negative control) and *sodB*, where
326 the enzyme activities increased about 2.5-fold. Since essentially all cellular processes
327 in *E. coli* are more efficient at 37°C than at 25°C, we typically do not consider induction
328 factors below three as significant. The *trxA* gene is an exceptional case. The gene is
329 transcribed from two alternative start sites, leading to a short (58 nucleotides) and a
330 long (98 nucleotides) 5'-UTR. As observed previously [14], only the 5'-UTR of the short
331 transcript contains a functional RNAT as shown by the beta-galactosidase activity and
332 protein increase in case of the short but not the long construct (Fig. 3B).

333 To determine the influence of these RNATs in the native background, we introduced
334 the translational fusions into *Y. pseudotuberculosis*. Here, only the 5'-UTRs of *katY*
335 and the short *trxA* transcript conferred translational repression at 25°C and induction
336 at 37°C, most prominently again for *katY* with a more than 20-fold change (Fig. 3C).

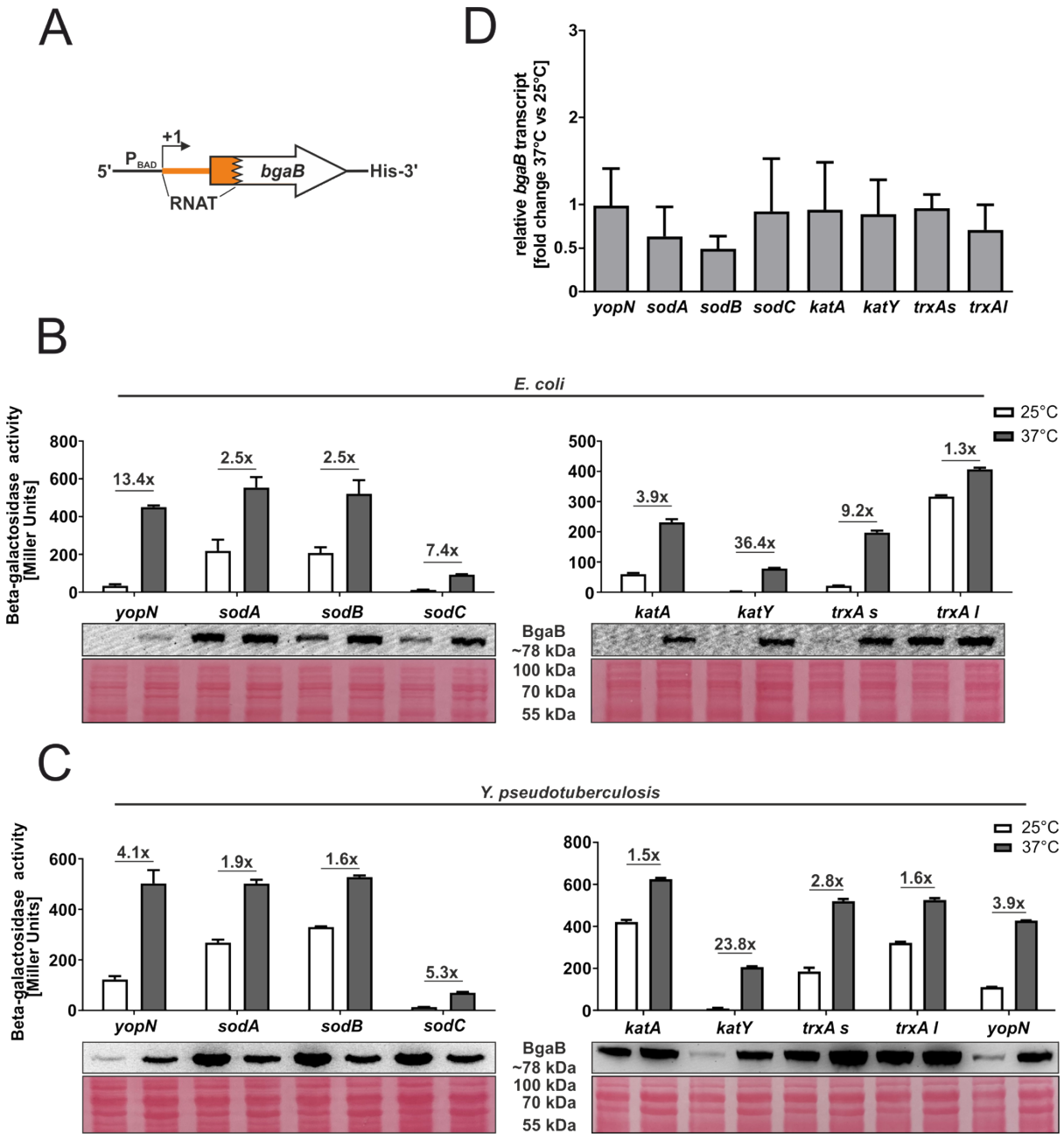

Figure 3. Translational control of *Y. pseudotuberculosis* ROS defense genes. (A) Schematic representation of the reporter gene fusion. The RNAT was translationally fused to the *bgaB* gene. Transcription was dependent on the pBAD promoter. As a control, the *yopN* RNAT was used. The fusion plasmids were introduced into *E. coli* (B) or *Y. pseudotuberculosis* YPIII cells (C) and grown to an OD_{600} of 0.5 at 25°C. Transcription from the pBAD promoter was induced by the addition of 0.01 % or 0.1 % L-arabinose in *E. coli* and *Y. pseudotuberculosis*, respectively. The cultures were split and incubated at 25 or 37°C. After 30 min, samples were taken for β-galactosidase assays, Western blot analysis and qRT-PCR. Experiments were carried out multiple times. Mean and corresponding standard deviation of biological triplicates are shown. Western blot membranes were stained with Ponceau S as a loading control. One representative Western blot is shown. (D) Levels of *bgaB* transcript determined by qRT-PCR from cells used in (C) were normalized to *gyrB* and *nuoB* mRNA amounts. The mean of three biological replicates and technical triplicates with their corresponding standard deviation are shown.

To ascertain that the mRNA levels derived from the pBAD promoter were roughly similar at 25 and 37°C, *bgaB* levels were determined by qRT-PCR using the same

Yersinia samples as in Fig. 3C. Comparison between 25 and 37°C showed almost equal mRNA levels for most constructs (Fig. 3D). Only the *sodA* and *sodB* fusions showed a reduced *bgaB* transcript amount at 37°C. Overall, these results support the hypothesis that the 5'-UTRs of several *Yersinia* ROS defense genes regulate translation initiation.

3.3 A stabilizing point mutation prevents RNAT regulation of the short *trxA* transcript

The *trxA* transcript caught our attention as it occurs in two isoforms of different lengths (Fig. 4A and B), of which only the short 5'-UTR acts as translational control element (Fig. 3). It folds into a structure that partially occludes the ribosome binding site (Fig. 4A). The unpaired adenosine residues in the SD sequence and the start codon might be responsible for the temperature responsiveness. Several reasons might account for the high expression of the long *trxA* variant already at low temperature. In contrast to the single mismatch in the SD sequence of the short isoform, the long one features two mismatched residues resulting in a kinked structure (Fig. 4B). In addition, the start codon in the long transcript is more accessible than in the short one. Altogether, these differences likely explain why the long version is unable to repress ribosome binding and translation initiation at low temperature.

To investigate the temperature-responsive RNA structure of the short *trxA* isoform in more detail, we constructed a stabilized version (rep) by replacing the unpaired adenine in the anti-SD sequence by an uracil resulting in a perfectly paired SD sequence (Fig. 4A). In the *bgaB* reporter system, the stabilizing mutation abolished expression both at low and at high temperatures in *E. coli* and in *Y. pseudotuberculosis* (Fig. 4C).

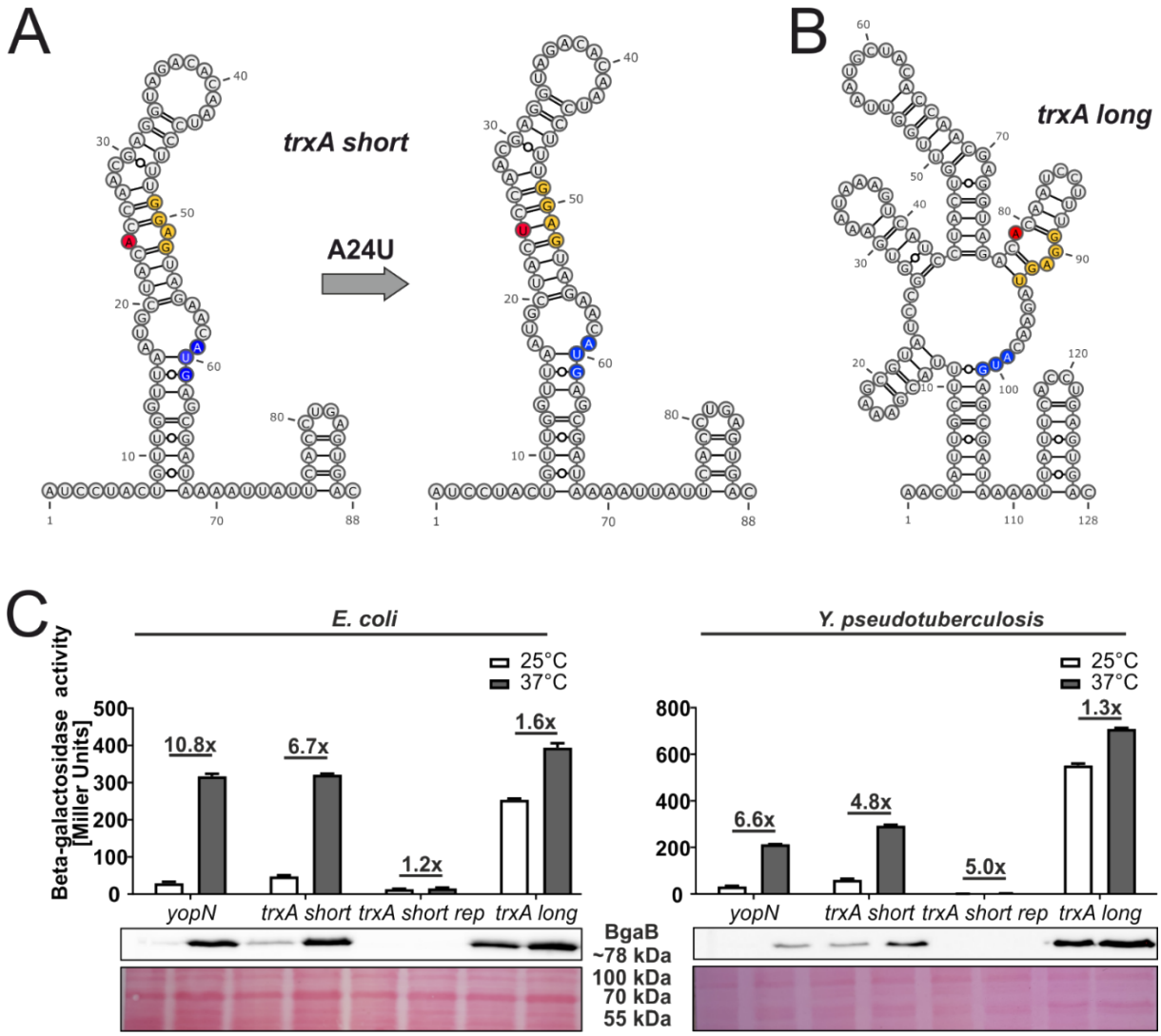

Figure 4. Only the 5'-UTR of the short *trxA* transcript contains a thermoresponsive RNA structure. PARS-derived secondary structure of the short **(A)** and long **(B)** *trxA* RNAT and its predicted stabilized structure after mutation of the anti-SD sequence. The SD sequence is highlighted in yellow, its corresponding start codon in blue and the mutation site in red. –, AU pair; =, GC pair; and ○, GU pair. **(C)** Translational control was measured by *bgaB* fusions under control of the pBAD promoter. The *yopN* RNAT served as positive control. Experiments were carried out as described in Fig. 3.

To solidify the claim that the short *trxA* RNA structure melts between the SD sequence and the start codon, we applied enzymatic RNA structure probing and treated *in vitro* transcribed 5'-end labeled RNA at different temperatures with RNases T1 (cuts unpaired guanines) and T2 (preferentially cuts unpaired adenines but also other unpaired nucleotides). In the wild-type (WT) RNA, we observed almost no cleavage around the SD sequence and the start codon at 25°C but prominent cleavage at 37

391 and 42°C consistent with thermally induced melting of these regions (Fig. 5A). In
392 accordance with the absence of any reporter gene activity (Fig. 4C), the same regions
393 in the rep variant were completely protected from ribonucleolytic attack indicating that
394 melting of the structure is prevented by locking the structure in a closed conformation
395 (Fig. 5A).

396 Finally, we tested the RNAs for their accessibility to ribosome binding by employing
397 primer extension inhibition (toeprinting) assays at different temperatures. The WT and
398 rep RNAs were reversely transcribed in the presence or absence of 30S ribosomal
399 subunits. The occurrence of prematurely terminated reverse transcripts (toeprints)
400 indicates successful binding of the 30S ribosome by acting as a roadblock for cDNA
401 synthesis. As expected, the WT *trxA* transcript generated a toeprint signal in the
402 presence of 30S subunits with increasing temperatures whereas the rep version did
403 not (Fig. 5B). Cumulatively, the *in vivo* and *in vitro* experiments provide compelling
404 evidence that the short *trxA* isoform contains a functional RNAT that is solely
405 responsible for temperature regulation since transcription of *trxA* is similar at 25 and
406 37°C in *Y. pseudotuberculosis* (Fig. 2).

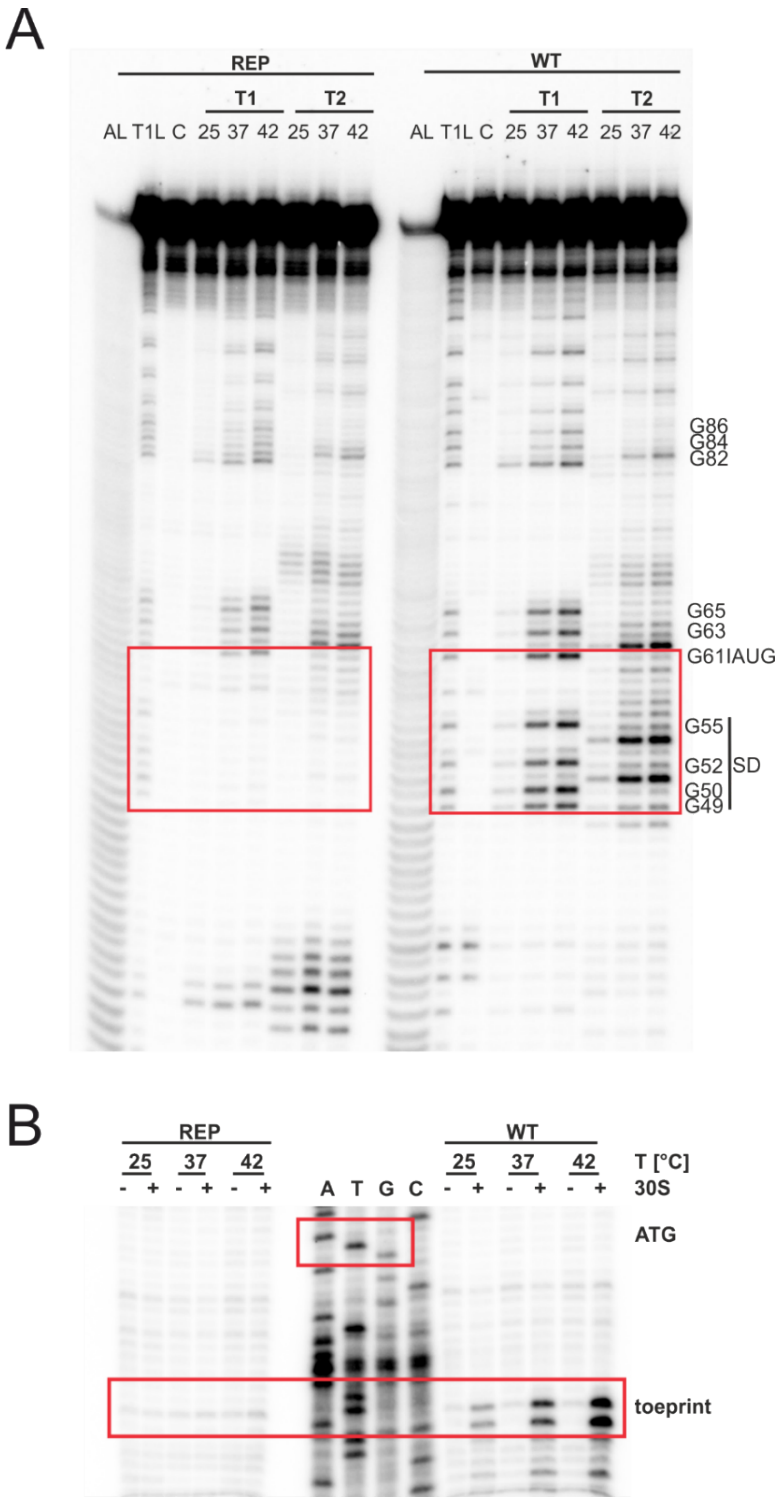

Figure 5. The short *trxA* RNAT melts at higher temperatures and facilitates ribosome binding. **(A)** Enzymatic structure probing of the short *trxA* RNAT (WT) and its stabilized version (REP). Radiolabelled RNA was treated with RNases T1 and T2 at 25, 37 and 42°C. AL, alkaline ladder; T1L, RNase T1 cleavage ladder in sequencing buffer at 37°C; C, RNA treated with water instead of RNases – cleavage control. The ribosome-binding site is highlighted by a red box. **(B)** Primer extension inhibition of the short *trxA* RNAT (WT) and its stabilized version (REP) was conducted at 25, 37° and 42°C with (+) and without (−) the addition of 30S ribosomal subunits. Ribosome binding leads to the accumulation of a toeprint signal. ATGC lanes indicate sequencing reactions for orientation. Position of ATG and the toeprint signal is highlighted by red boxes. Experiments were carried out at least twice.

3.4 Stabilizing mutations in the 5'-UTRs of *sodB*, *sodC* and *katA* impair regulation

Despite initial evidence for RNATs in the *sodB* and *sodC* (but not *sodA*) transcripts by global RNA structure profiling through parallel analysis of RNA structures (PARS) and reporter gene assays in *E. coli* [14], the results presented in Fig. 3 raised doubts whether they function as thermosensors in *Y. pseudotuberculosis*. We wanted to understand this discrepancy and constructed repressed versions of the *sodB* and *sodC* 5'-UTRs by introducing stabilizing point mutations in the anti-SD region (Fig. 6A and 6B). As an indication that the WT structure has a functional role, the mutated versions prevented translation at both temperatures in *E. coli* and *Y. pseudotuberculosis* (Fig. 6C).

Consistent with this assumption, *in vitro* transcribed RNA showed a temperature-induced melting around the RBS whereas the same region in the mutated RNA was protected from ribonuclease even at 42°C except for the bulged nucleotide G85 (Fig. 7A). Accordingly, toeprinting revealed ribosome binding to the WT *sodB* RNAT at 37 but not at 25°C, and no toeprint signal was observed for the stabilized version (Fig. 7B). Similar observations were made when the *sodC* 5'-UTRs (WT and rep variant) were subjected to structure probing (Fig. 7C) and toeprinting (Fig. 7D). Altogether, these biochemical experiments support the idea that the *sodB* and *sodC* 5'-UTRs are able to melt in response to increasing temperature to permit ribosome binding. In *Yersinia*, however, this response seems to be dampened by yet unknown mechanisms.

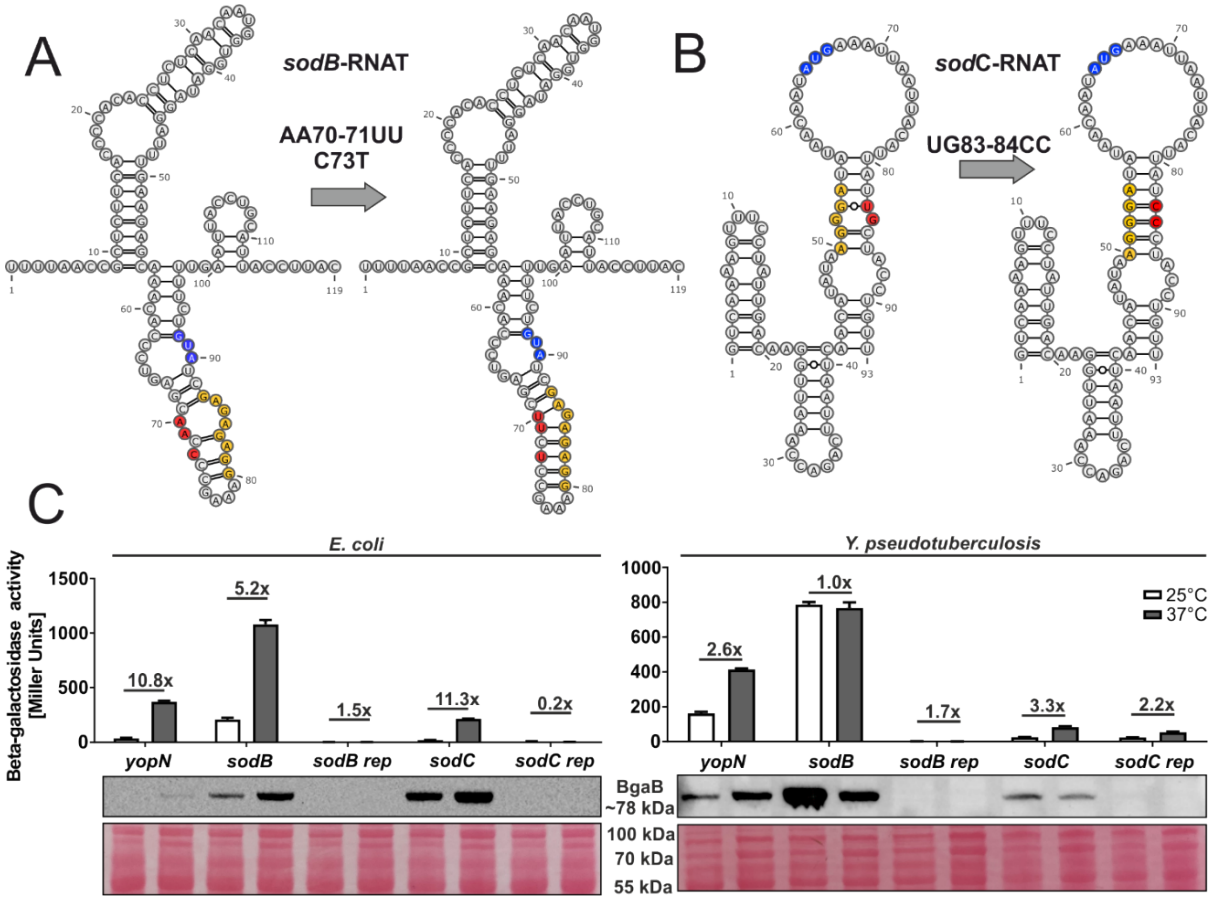

Figure 6. The 5'-UTRs of the *sodB* and *sodC* transcripts contain a thermoresponsive structure. PARS-derived secondary structure of the *sodB* RNAT (A) and the MFE structure of the *sodC* RNAT (B) with their corresponding predicted stabilized structure after mutation of the anti-SD sequence. The SD sequence is highlighted in yellow, the AUG codon in blue and the mutation site in red. –, AU pair; =, GC pair; and ○, GU pair. (C) Translational control was measured by *bgaB* fusions. The RNAT was translationally fused to *bgaB* under control of the pBAD promoter. The *yopN* RNAT was used as positive control. Experiments were carried out as described in Fig. 3.

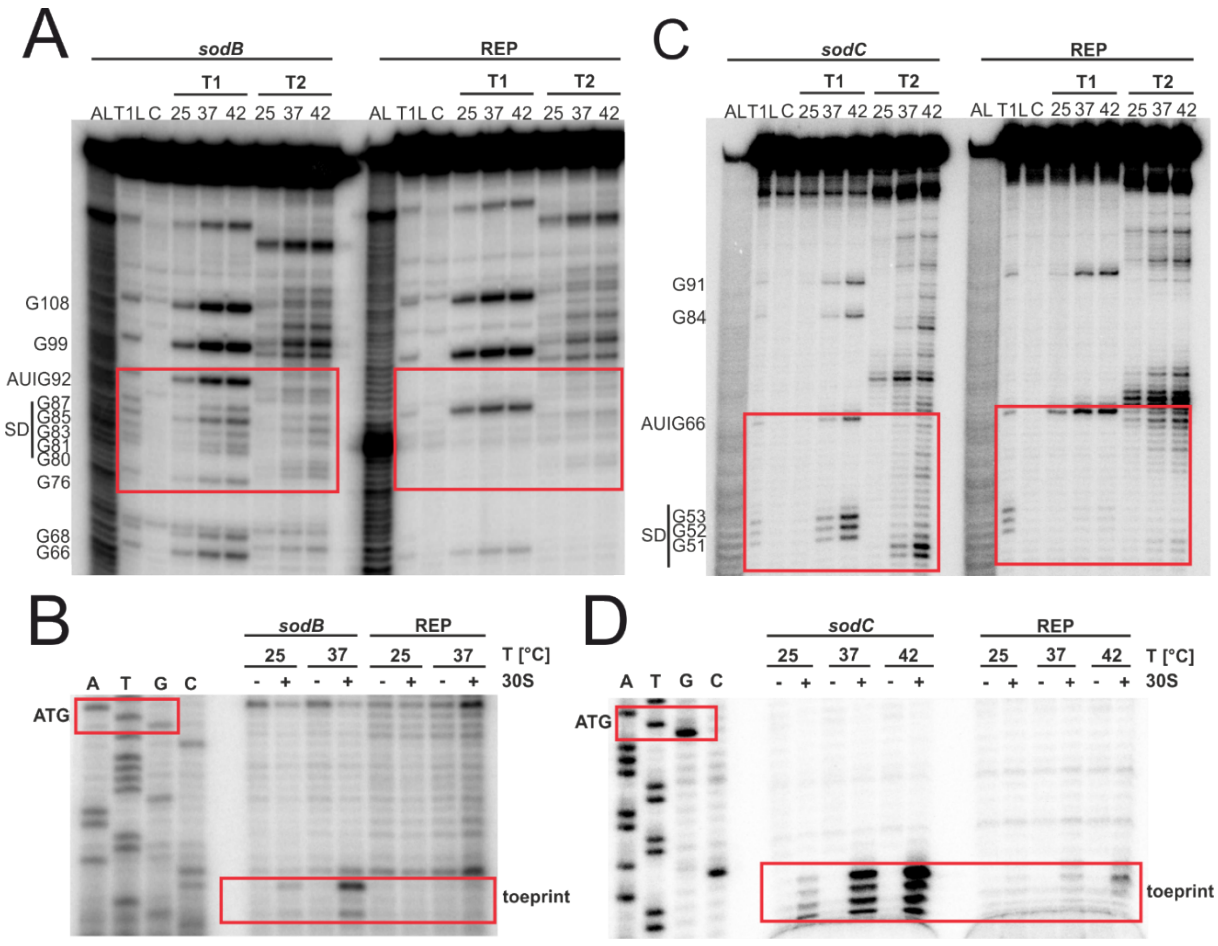

Figure 7. Structure probing and toeprinting support temperature-responsive melting and ribosome binding to the *sodB* and *sodC* 5'-UTRs. Enzymatic structure probing of the *sodB* **(A)** and *sodC* **(C)** RNATs and their stabilized version (REP). Radiolabelled RNA was treated with RNases T1 and T2 at 25, 37 and 42°C. AL, alkaline ladder; T1L, RNase T1 cleavage ladder in sequencing buffer at 37°C; C, RNA treated with water instead of RNases – cleavage control. The ribosome-binding site is highlighted by a red box. Primer extension inhibition of the *sodB* **(B)** and *sodC* **(D)** RNATs and their stabilized version (REP) was conducted at 25, 37° and 42°C with (+) and without (−) the addition of 30S ribosomal subunits. Ribosome binding leads to the accumulation of a toeprint signal. ATGC lanes indicate sequencing reactions for orientation. Position of ATG and the toeprint signal is highlighted by red boxes. Experiments were carried out at least twice.

Likewise, we wanted to understand the observed difference in the behaviour of the *katA* 5'-UTR in *E. coli* and *Y. pseudotuberculosis* (Fig. 3). Due to the nature of the RNA structure with the SD sequence in a terminal loop (Fig. 8A), we did not change the anti-SD sequence but stabilized the adjacent hairpin structure by changing the unpaired adenosine and cytosine at position 109 and 110 into a cytosine and guanine, respectively. In the reporter gene assay, we observed the expected effect of

translational repression in *E. coli* and *Y. pseudotuberculosis* (Fig. 8B). By RNA structure probing, we could further show that the 5'-UTR of *katA* melts at higher temperatures, not only between the SD sequence and the start codon, but also further downstream. According to the PARS profiles at different temperatures, the nucleotides 130-136 should primarily be in a single-stranded conformation prone to RNase cleavage at 25°C [14]. As these residues were partially protected from T1 and T2 attack at low temperature, they are probably engaged in a more complex overall structure. As expected, the rep variant showed almost no cleavage around the entire RBS suggesting substantial stabilization due to the formation of an improved hairpin structure (Fig. 8C). Consistent with the probing results, a toeprint signal was found at 37°C with the WT *katA* RNA, but not with the REP version (Fig. 8D). Instead, other premature termination products of reverse transcription were found, which often occur near stable structures in stabilized RNATs [11]. Like *sodB* and *sodC*, the *katA* 5'-UTR appears to be capable of thermally controlling access to the SD sequence, but the dynamic nature of these RNA structures seems to play a minimal role in the *Yersinia* cell under the tested conditions.

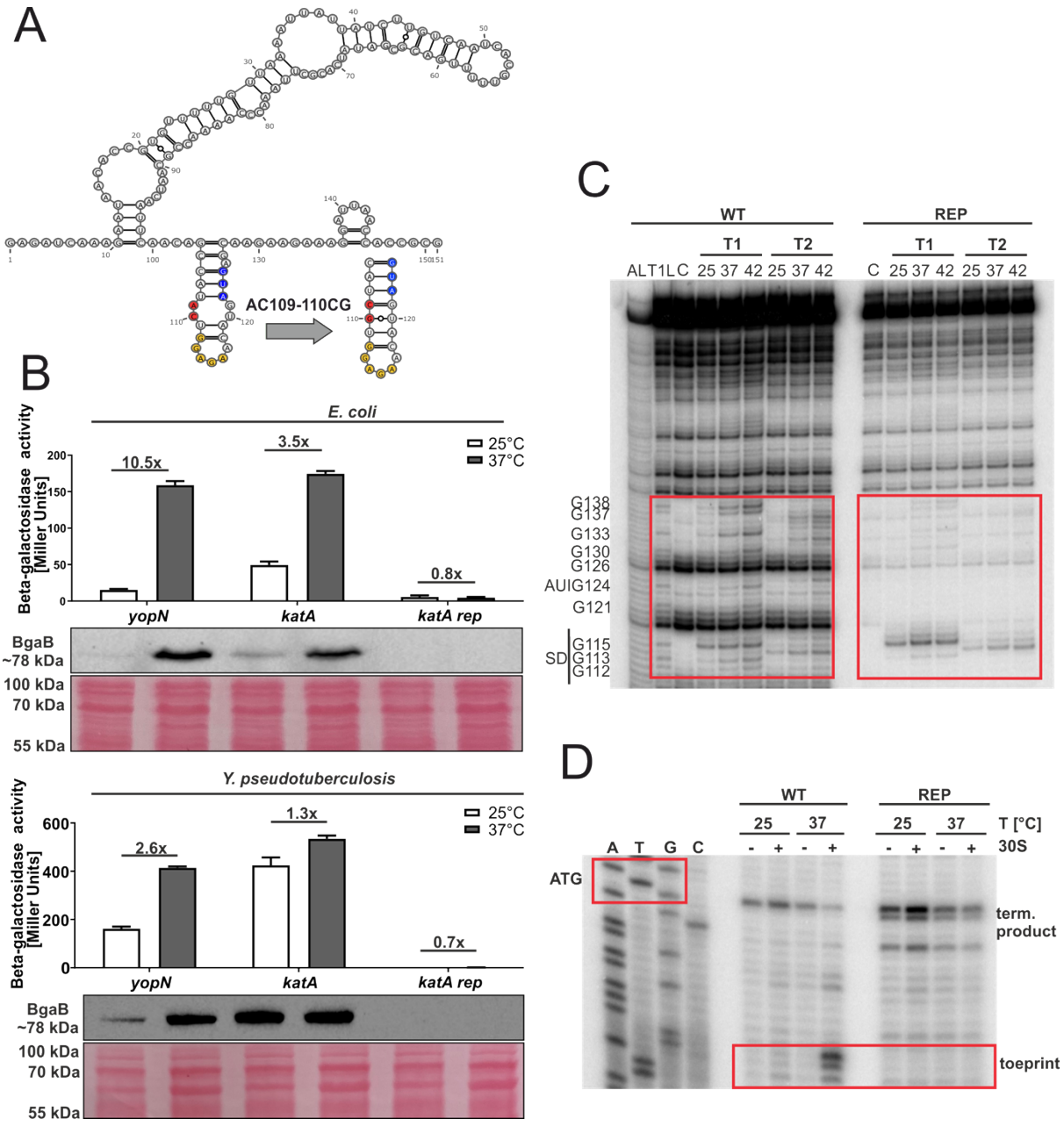

Figure 8. The 5'-UTR of the *katA* transcript contains a thermoresponsive structure. (A) PARS-derived secondary structure of the *katA* RNAT with its predicted stabilized structure after mutation of a loop in the RBS to create a hairpin structure. The potential SD sequence is highlighted in yellow, its corresponding AUG in blue and the mutation site in red. –, AU pair; =, GC pair; and ○, GU pair. **(B)** Translational control was measured by *bgaB* fusions. The RNAT was translationally fused to *bgaB* under control of the pBAD promoter. As a control the *yopN* RNAT was used. Experiments were carried out as described in Fig. 3. **(C)** Enzymatic structure probing of the *katA* RNAT (WT) and its stabilized version (REP). Radiolabelled RNA was treated with RNases T1 and T2 at 25, 37 and 42°C. AL, alkaline ladder; T1L, RNase T1 cleavage ladder in sequencing buffer at 37°C; C, RNA treated with water instead of RNases – cleavage control. The ribosome-binding site is highlighted by a red box. **(D)** Primer extension inhibition of the *katA* RNAT (WT) and its stabilized version (REP) was conducted at 25, 37°C, with (+) and without (−) the addition of 30S ribosomal subunits. Ribosome binding leads to the accumulation of a toeprint signal. ATGC lanes indicate sequencing reactions for orientation. Position of ATG and the toeprint signal is highlighted by red boxes. Experiments were carried out at least twice.

3.5 The *katY* 5'-UTR harbors an RNAT that is functional in *Y. pseudotuberculosis*

The most prominent temperature response of all ROS defense mRNAs was observed in the case of *katY* (Fig. 3). The 5'-UTR of *katY* had escaped our attention as an RNAT candidate in previous RNA structuromic approaches because most of the sequence relevant for masking the RBS is not located in the 5'-UTR but within the coding sequence (Fig. 9A). To characterize this new RNAT candidate, we generated structural mutants. A stabilized version (U31C) was constructed by exchanging a weak UG pair in the SD/anti-SD region by a stronger CG pair. This variant completely repressed translation at 37°C (Fig. 9B). Introduction of an additional mutation (UA31-32CU; Fig. 9A) initially aimed at stabilizing the structure even further, was predicted to result in a structural re-arrangement that slightly derepressed RNAT activity (Fig. 9B). To exclude that these regulatory effects were due to changes in the mRNA levels, we compared the *bgaB* levels from the *Y. pseudotuberculosis* samples used in Fig. 9B by qRT-PCR and detected no significant differences between 25 and 37°C (Fig. 9C). In further support of a translational control mechanism, we observed increased sensitivity to RNase cleavage around the SD sequence and the start codon at higher temperatures in structure probing experiments (Fig. 9D) and increased binding of the ribosome at higher temperatures in toeprinting assays (Fig. 9E). All these results demonstrate that the *katY* 5'-UTR harbors a *bona fide* RNAT.

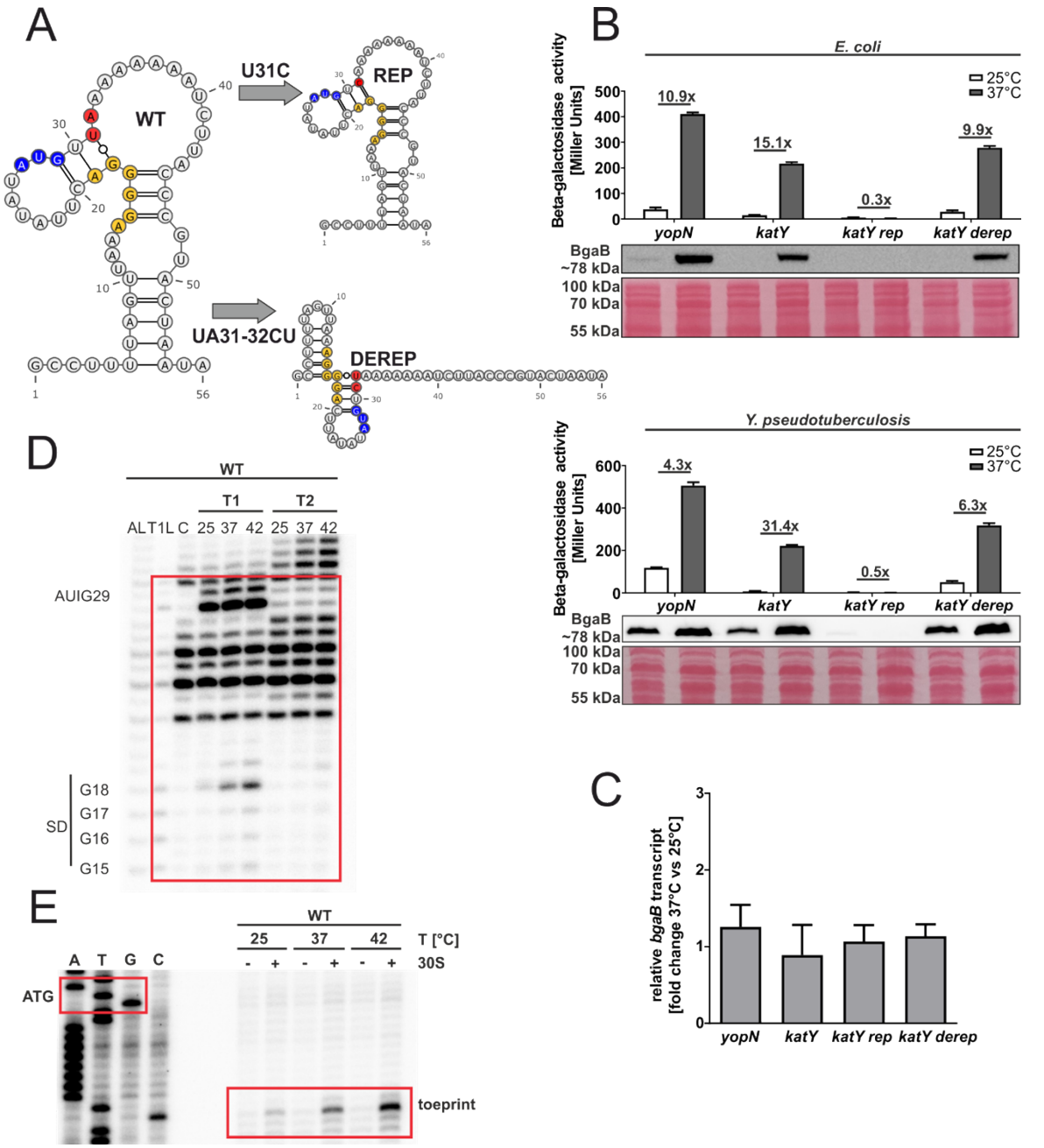

Figure 9. The *katY* 5'-UTR is a functional RNAT *in vitro* and in *Y. pseudotuberculosis*. PARS-derived secondary structure of the *katY* **(A)** RNAT with its predicted stabilized (REP) and destabilized structure (DEREP) after mutation of the anti-SD sequence. The potential SD sequence is highlighted in yellow, its corresponding AUG in blue and the mutation site in red. –, AU pair; =, GC pair; and ○, GU pair. **(B)** Translational control was measured by *bgaB* fusions. The RNAT was translationally fused to *bgaB* under control of the pBAD promoter. As a control the *yopN* RNAT was used. Experiments were carried out as described in Fig 3. **(C)** Levels of *bgaB* transcript determined by qRT-PCR from *Y. pseudotuberculosis* cells used in **(B)** were normalized to *gyrB* and *nuoB* mRNA amounts. The mean of three biological replicates and technical triplicates with their corresponding standard deviation are shown. **(D)** Enzymatic structure probing of the *katY* RNAT (WT). Radiolabelled RNA was treated with RNases T1 and T2 at 25, 37 and 42°C. AL, alkaline ladder; T1L, RNase T1 cleavage ladder in sequencing buffer at 37°C; C, RNA treated with water instead of RNases – cleavage control. The ribosome-binding site is highlighted by a red box. **(E)** Primer extension inhibition of the *katY* RNAT (WT) was conducted at 25, 37°C, with (+) and without (−) the addition of 30S ribosomal subunits. Ribosome binding leads to the accumulation of a toeprint signal. ATGC lanes indicate sequencing reactions for orientation. Position of ATG and the toeprint signal is highlighted by red boxes. Experiments were carried out at least twice.

3.6 Temperature affects the susceptibility of *Y. pseudotuberculosis* against H_2O_2

The upregulation of *katA* expression at 37°C on the transcriptional level (Fig. 2) and – more prominently – *katY* expression on both the transcriptional and translational level (Fig. 2, 3C and 9B), lead us to believe that *Yersinia* cells might be better protected against ROS when grown at 37°C instead of 25°C. To test this hypothesis and to dissect the contribution of individual players to ROS detoxification, we generated markerless catalase deletion mutants and tested their susceptibility to H_2O_2.

First, we conducted a zone of inhibition assay with *Yersinia* cells pre-grown at 25 or 37°C and spread onto agar plates. The bacteria were then subjected to a diffusion gradient of H_2O_2 from a paper disk, and the plates were incubated at 25 or 37°C. Congruent with our hypothesis of a better protection at elevated temperatures, we observed a significantly reduced zone of inhibition for the wildtype (WT) strain, if it was grown at 37 compared to 25°C (Fig. 10A). The zone of inhibition at both temperatures became larger when the *katA* gene was removed (Δ*katA*), indicating a general protective effect against H_2O_2 as expected for a catalase gene. Deletion of the *katY* gene (Δ*katY*) did not increase the zone of inhibition at 25°C compared to the WT. Strikingly, the zone of inhibition remained unchanged at 37°C suggesting that the temperature-induced protection in the WT and Δ*katA* strains is mediated by KatY. Deletion of both catalase genes (ΔΔ*katAY*) resulted in a combined phenotype of the single mutants with an increase in the zone of inhibition and no reduction at 37°C.

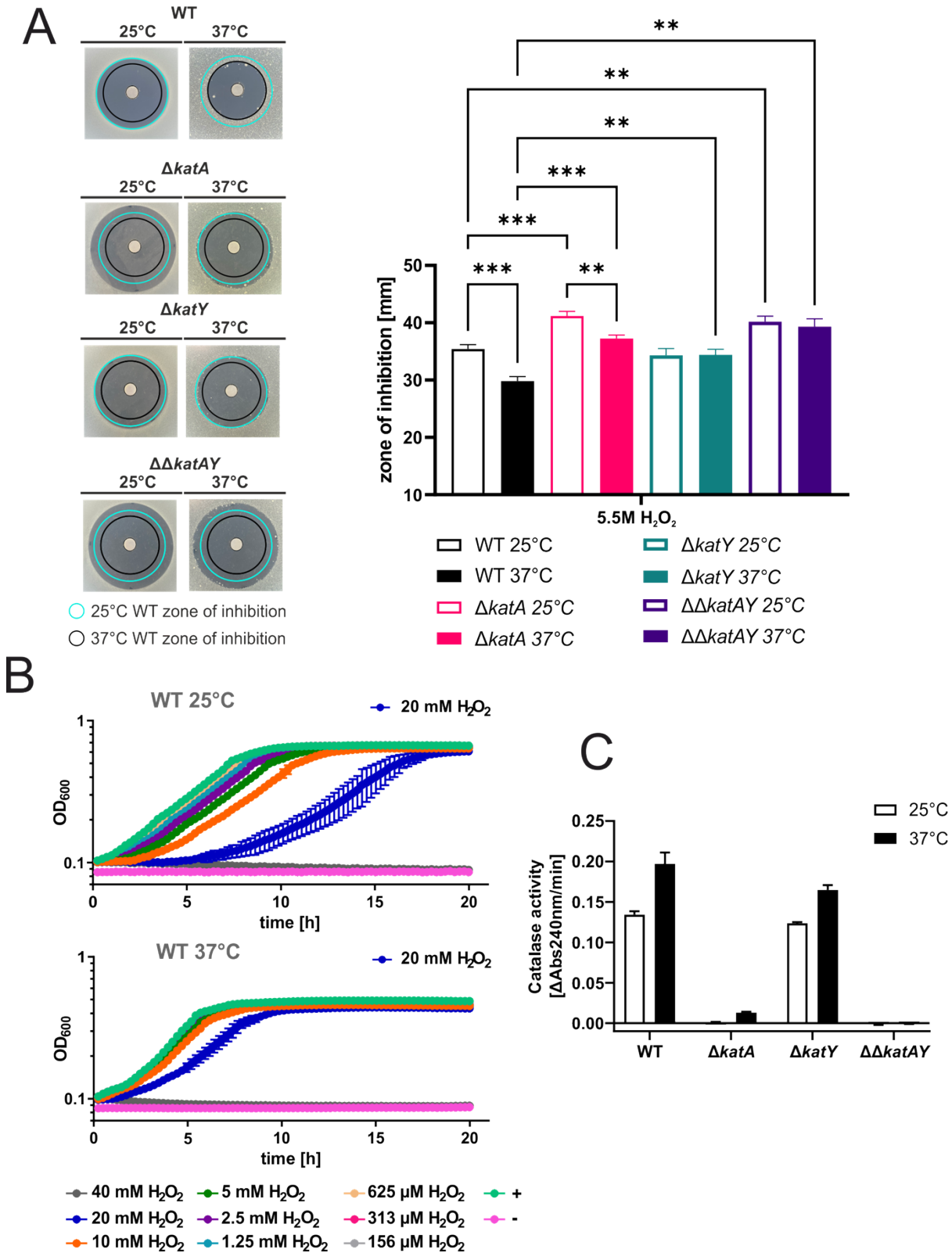

Figure 10. Temperature-dependent influence of *katA* and *katY* on the oxidative stress response in *Y. pseudotuberculosis*. (A) Disk diffusion assay for H_2O_2 was conducted by applying 3 µl of 5.5 M H_2O_2 onto paper disks on soft agar containing a bacterial suspension. After 24 h of growth at the indicated temperature the zone of inhibition was measured. The experiment was carried out multiple times and each time in biological triplicates and two technical replicates. Cyan ring = zone of inhibition measured for the wildtype at 25°C. Black ring = zone of inhibition measured for the wildtype at 37°C. Asterisks indicate statistically significant differences by oneway ANOVA (n = 3; * p < 0.05; ** p < 0.01;

*** p < 0.001) **(B)** Cells were pre-grown at 25°C or 37°C and diluted to an OD_{600} of 0.05 in a 96 well plate. H_2O_2 was added to the indicated final concentrations. Growth was monitored by measuring the OD_{600} during incubation at 25°C or 37°C. The highest concentration, which allowed growth is highlighted. + = no H_2O_2 control, - = medium control. The mean and the standard deviation of biological triplicates are plotted. Experiments were carried out multiple times. **(C)** Decomposition of H_2O_2 was measured in real-time by reading the absorption of H_2O_2 at 240 nm over time at 25°C. Cells were grown at 25°C or 37°C until an OD_{600} of 0.5 was reached. Cells were lysed by ultrasonication. Lysate with a protein concentration of 50 µg/ml, determined by Bradford assay, was used and treated with 0.01 M H_2O_2. The velocity of H_2O_2 decomposition was calculated based on the linear range at the beginning of the curve. The mean and standard deviation are shown. Experiments were carried out at least twice in biological triplicates.

Next, we tested if these observations hold true in liquid culture by conducting growth experiments under various H_2O_2 concentrations and observed similar results, showing reduced susceptibility against H_2O_2 at 37°C and a prominent KatY effect (Fig. 10B and Fig. S1). Finally, we examined whether protection is due to catalase activity and performed an activity assay testing the ability of cell lysates generated from cells grown at 25 or 37°C to decompose H_2O_2. This assay measures the absorbance of H_2O_2 directly by UV-light [31]. Hence, catalase activity correlates with the reduction of absorbance. Consistent with the phenotypes described above, we observed a higher catalase activity if *Yersinia* WT cells were grown at 37°C compared to 25°C (Fig. 10C). The Δ*katA* mutant, which can only produce KatY, shows essentially no activity at 25°C but weak activity at 37°C. The catalase activity of the Δ*katY* mutant at 25°C was similar to the WT activity suggesting KatA to be the only catalase present at 25°C. The increase at 37°C was slightly lower than in the WT. Adding up the activities of both catalases measured at 37°C in the single mutants resulted in a value similar to the WT activity. As expected, the double mutant ΔΔ*katAY* did not exhibit any catalase activity at all.

Complementing the deletion strains by reintroducing the catalase genes into their native genomic context by homologous recombination restored the corresponding

phenotypes (Fig. S2A, S3) and catalase activities (Fig. S2B). The reintegrated catalase genes encoded a C-terminal His-tag, which allowed us to quantify the KatA and KatY protein amounts at 25 and 37°C. KatA was present at almost equal amounts at both temperatures in all complemented backgrounds (Fig. 11). KatY, however, was barely detectable at 25°C and strongly increased at 37°C, which supports the hypothesis that KatY is the primary temperature-regulated catalase in *Y. pseudotuberculosis*. At least one shorter KatY product was detected in all immunoblots. It presumably represents a truncated KatY derivative as it has been described in *Y. pestis* [22].

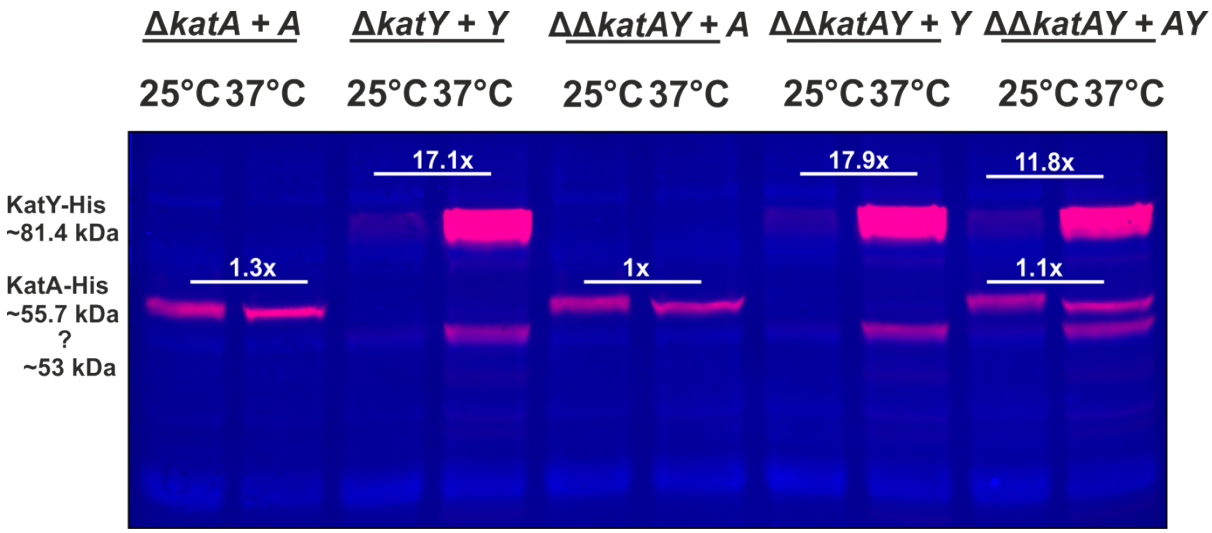

Figure 11. KatY is the major temperature-regulated catalase in *Y. pseudotuberculosis*. The deletion strains were complemented by homologous recombination with C-terminal His-tagged KatA and KatY proteins. Cells were grown to an OD_{600} of 0.5 at 25 and 37°C. Samples were loaded on TGX-Stain-Free gels and the protein amount was quantitatively analysed by fluorescence detection. Normalization to the total protein amount was achieved by Stain-Free visualization. The overlay of the fluorescent detection with the Stain-Free visualisation of the total protein amount of one representative Western blot is shown. Fold differences represent the mean of three biological replicates.

In an independent line of complementation experiments, we produced the KatY-His protein from a plasmid under control of the arabinose inducible pBAD promoter. Here also, KatY levels were upregulated at 37°C, no matter how strongly transcription was enforced by different arabinose concentrations (Fig. S4). In perfect agreement with the

results from the *bgaB* fusions, this finding supports the assumption that *katY* expression is to a large extent translationally controlled by an RNAT.

3.7 Temperature regulated *katY* expression affects H_2O_2 detoxification and intracellular redox state

To further elucidate the interplay between KatA and KatY in temperature-regulated ROS protection, we employed the genetically encoded redox-sensitive probe roGFP2-Orp1, an H_2O_2-sensitive variant of roGFP2. The roGFP2 protein carries redox-sensitive cysteines and is a reliable sensor for the intracellular redox-state [32]. roGFP2 has many advantages compared to redox-sensitive fluorescent dyes. For example reversibility, the ability to be genetically targeted into specific cell compartments, and most importantly its quantitative nature due to a ratiometric approach, which compensates for differences of roGFP2 concentration [29]. Here, we used roGFP2-Orp1, which is fused to the oxidant receptor peroxidase Orp1 from yeast, enabling specific and sensitive real-time measurement of intracellular H_2O_2 through the efficient proximity-based peroxidase redox relay [29,33]. H_2O_2 causes oxidation of the Orp1 thiol groups leading to the formation of disulfide bonds (Fig. 12A). Oxidized Orp1 promotes oxidation of the thiol groups of roGFP2 due to its close proximity leading to the formation of disulfide bonds at the roGFP2 protein. This formation induces a small conformational change in the protein resulting in a shift in the excitation spectrum. Under reduced conditions (untreated or DTT; dithiothreitol treated), roGFP2 exhibits an excitation peak at around 480 nm. Upon thiol oxidation (e.g., by AT-2; 2,2′-Dipyridyl disulfide treatment), the intensity of this peak is reduced and another excitation peak at around 400-405 nm appears (Fig. 12B). By calculating the ratio between these peaks and normalizing it to the mean ratios of fully oxidized

641 (AT-2) and fully reduced (DTT) probes over the course of the experiment, the

642 normalized ratio OxD is calculated [30].

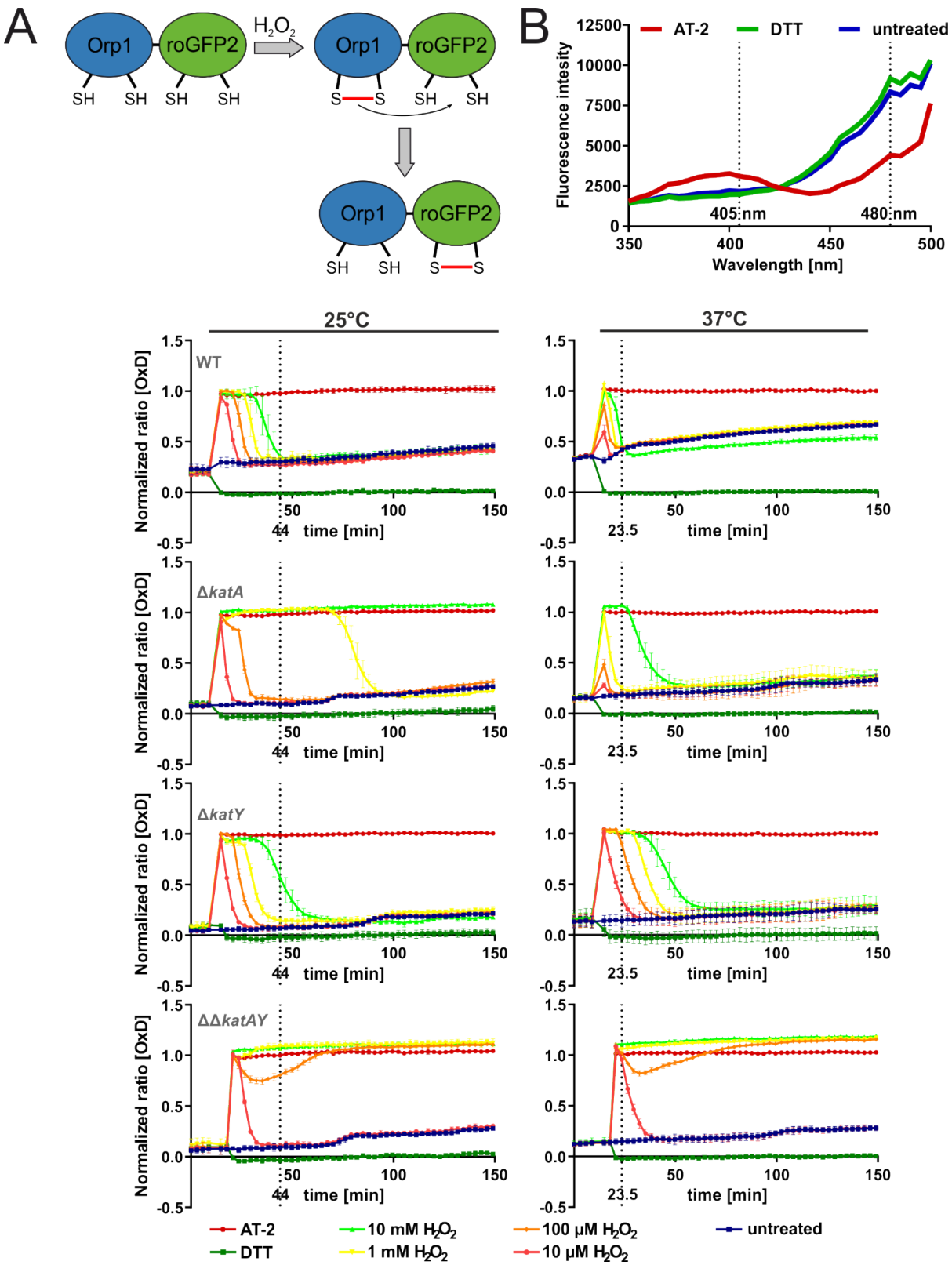

643

Figure 12. KatY is responsible for the temperature dependent H_2O_2 detoxification at the intracellular level. Cells expressing the redox-sensitive roGFP2-Orp1 probes at 25°C or 37°C were washed with PBS and diluted to an OD_{600} of 0.2 and 100 µl were transferred to a black 96 well plate. The fluorescence intensity at 405 nm and 488 nm was recorded over 150 min at room temperature. After measuring for 10 minutes, AT-2, DTT and H_2O_2 were added. The normalized ratio of 405/488 nm is plotted. A ratio of 1 indicates full oxidation and a ratio of 0 indicates full reduction of the probe. The dotted line indicates the timepoint at which all H_2O_2 treated wildtype cells are returned to their untreated state. The mean and the standard deviation of biological triplicates are plotted. Experiments were carried out multiple times.

Y. pseudotuberculosis cells harboring the roGFP2-Orp1 fusion plasmid were grown at 25 or 37°C. Upon reaching the early exponential phase, expression of the redox probe was induced by addition of IPTG before cultures were grown at 25 or 37°C overnight. Sufficient production and functionality of roGFP2-Orp1 was checked by measuring the excitation spectrum after addition of AT-2 and DTT. DTT, as a reductant, will fully reduce roGFP2-Orp1, while the oxidant AT-2 fully oxidizes roGFP2-Orp1 giving a readout of maximum probe reduction and oxidation before conducting the experiments. Fresh bacterial cells were then treated with AT-2, DTT or different H_2O_2 concentrations and directly measured for changes in their redox state at room temperature. The redox probe rapidly and fully oxidized after H_2O_2 application in the WT cells grown at 25°C. Over time, the signals returned to the untreated level, reaching it after 44 min at the highest concentration of H_2O_2 (Fig. 12C). In contrast, in the WT grown at 37°C, the probe already returned to the untreated level at 23.5 min. Furthermore, lower H_2O_2 concentrations were not sufficient to fully oxidize the probe in cells grown at 37°C, suggesting an increased protection of the intracellular space and a faster removal of H_2O_2 when compared to 25°C. Consistent with the phenotypic characterization described above, the Δ*katA* mutant showed higher susceptibility against H_2O_2. The Δ*katA* cells grown at 25°C were no longer able to reduce roGFP2-Orp1 after addition of 10 mM H_2O_2. At 37°C, better protection against H_2O_2 was observed. Here, low H_2O_2 concentrations did not lead to full oxidation of roGFP2-Orp1,

and eventually the probe is re-reduced to the untreated level with all H_2O_2 concentrations. The Δ*katY* strain showed a response similar to the WT at 25°C, but interestingly unlike the WT, no increase in the cells capability to detoxify H_2O_2 was observed in this mutant. Since the double deletion strain ΔΔ*katAY* lacks both catalases, it shows the lowest capacity to detoxify H_2O_2 and to re-reduce the probe. Based on our observations that the Δ*katA* strain improves its H_2O_2 resistance at 37°C and the Δ*katY* strain, while resilient as the WT at 25°C, is not increasing its detoxification capacity at 37°C. We conclude that the increased protection against H_2O_2 at 37°C originates from the temperature induced KatY protein.

4 Discussion

Enteric pathogens, like *Y. pseudotuberculosis,* need to quickly sense and adapt to their changing environment upon infection. A sudden temperature upshift is among the most stable cues indicating entry into a warm-blooded host. There are many ways how bacteria can sense and respond to temperature changes. One of them is the upregulation of transcription by temperature-dependent changes in the DNA topology, increasing the binding affinity of RNA polymerase to the promoter [34]. Increased transcription can be triggered by temperature dependent DNA-binding proteins such as the Histone-like nucleoid structuring protein H-NS [35]. In *Y. pseudotuberculosis*, H-NS forms a complex with the small YmoA protein and silences expression of *lcrF* coding for the virulence master regulator outside the host [36,37]. Another efficient way to directly modulate gene expression in response to increasing temperatures are RNATs. Here, the mRNA is already present in the cell and ready to be translated

[38,39]. Over the last decades, multiple RNATs have been described in various bacterial pathogens [11,40–44].

In this study, we followed up on previous reports showing that transcription and translation of several *Yersinia* ROS detoxification genes are induced at host body temperature [13–15]. Since the generation of reactive oxygen and nitrogen species constitutes the first line of host defense against microbial pathogens [45], a direct correlation between a temperature of 37°C and ROS defense gene expression in *Yersinia* is highly plausible. Here we aimed at understanding the underlying mechanistic details of this correlation for several classes of ROS detoxification genes.

Antioxidants, like thioredoxins are important to maintain a reduced intracellular state of proteins and remove the formed disulfide bonds, after ROS exposure [6]. In their reduced form, they can catalyze the reduction of protein disulfides and get oxidized themselves in the process. Subsequent reduction is facilitated by the thioredoxin reductase TrxB, with help of reducing equivalents from NADPH (Fig. 1) [46,47]. While there is no evidence for temperature regulated transcription of the *trxA* gene, we found clear evidence for translational control of the shorter of two *trxA* transcripts. The PARS calculated RNA structures [14] show a typical RNAT-like hairpin structure with internal bulges and loops in the short 5'-UTR (Fig. 4A). Stabilizing the SD/anti-SD interaction by exchange of just one residue impaired translational control, a clear indication that melting of the WT structure facilitates translation initiation, which was supported by *in vitro* experiments. The 5'-UTR of the long *trxA* adopts an entirely different structure that is unable to repress translation at 25°C presumably accounting for sufficient TrxA levels outside of the host. The reverse is true for the *Pseudomonas aeruginosa* quorum sensing gene *pqsA* gene. Here, the longer of two alternative transcripts

722 contains an extended 5‘-end capable of folding into an RNA structure that blocks
723 translation initiation [48]. We assume that the two different *trxA* start sites contribute
724 to balancing TrxA levels according to the environmental situation. Previous
725 transcriptome studies showed that the short *trxA* transcript is higher expressed than
726 the longer *trxA* transcript (Fig. S6) [13]. Therefore, a high level of TrxA is guaranteed
727 at 37°C due to the RNAT functionality of the 5’-UTR of the short *trxA* transcript.

728 Superoxide dismutases (SODs) are another important defense system when bacteria
729 face ROS challenges. *Y. pseudotuberculosis* encodes three types of SODs, an iron-
730 containing SodB [49], a manganese-containing SodA [49,50] and a copper-containing
731 SodC, which plays a role in *Yersinia* virulence in the *Galleria* model [51]. We expected
732 SodB and SodC to be induced at 37°C due to moderately increased mRNA amounts
733 and potential RNATs in their 5’-UTRs (Fig. 2, 3 and 6). Consistent with the previous
734 PARS analysis [14], a global *in vitro* RNA structure probing approach, our biochemical
735 data supported the existence of these RNATs (Fig. 7). Reporter gene fusions,
736 however, showed some temperature regulation in *E. coli* but essentially no repression
737 at 25°C in *Y. pseudotuberculosis*. Here, it is conceivable that additional post-
738 transcriptional mechanisms come into play to coordinate appropriate *sod* gene
739 expression. One known example in *E. coli* is the interaction of the small regulatory
740 RNA (sRNA) RyhB, a key player in iron homeostasis [52]. RyhB negatively affects
741 *sodB* expression by binding to the RBS of *sodB*, thereby blocking translation and
742 facilitating cleavage by RNase E and RNase III [53,54]. RyhB expression is controlled
743 by the ferric uptake repressor protein Fur [55], which negatively regulates RyhB
744 expression in the presence of iron. Since iron elicits oxidative stress due to the Fenton
745 reaction [56], an sRNA such as RyhB might perhaps help reduce the availability of
746 iron-sulfur cluster proteins, like SodB, inside the microbial pathogen at 37°C. In *Y.*

pestis and *Y. pseudotuberculosis* the involvement of iron availability was investigated. When grown in human plasma, which represents iron-limiting conditions and compared to growth in LB media, an upregulation of *sodA* and a downregulation of *sodB* was observed [49,57]. Another report adds to the relevance of metal ions in the protection against ROS induced damage. *Y. pseudotuberculosis* uses an unconventional way to combat ROS by importing zinc as antioxidant by secretion of a zinc-binding protein via the type VI secretion system (T6SS) [58,59].

Apart from currently unexplored sRNAs in the *Yersinia* oxidative stress response, even slightly different intracellular milieus in *E. coli* and *Y. pseudotuberculosis* or the fairly dilute conditions in the test tube might explain the observed differences between different experimental setups. It is well known that inorganic and organic cations or molecular crowding effects in the dense cellular environment can have profound effects on the folding and dynamic behavior of RNA structures [60–62].

Finally, and most importantly, we examined the temperature regulation of *Yersinia* catalases and discovered a massive upshift of KatY at 37°C primarily due to translational control by a novel RNAT. Catalases protect organisms against H_2O_2 toxicity by catalyzing its conversion into water and oxygen. KatA (also called KatE) and KatY (also called KatG) are distinct H_2O_2 scavenging systems. In *Y. pestis*, KatA is a monofunctional catalase functioning as primary scavenger for high levels of H_2O_2 whereas the bifunctional catalase/peroxidase KatY protein only shows marginal catalase activity [21]. KatY of *Y. pseudotuberculosis* is almost identical to its close relative in *Y. pestis* (99.86%). The *Y. pestis* KatY protein exists in multiple forms, most prominently an α-KatY form with a molecular mass of 78.8 kDa after processing of its leader signal sequence and a shorter β-KatY form with a molecular mass of 53.6 kDa

771 resulting from a secondary translational start signal [22,23]. An equivalent secondary
772 translation start site and similar translation products were observed in *Y.*
773 *pseudotuberculosis* (Fig. 11) supporting the close relationship between these two
774 species.

775 Given this kinship, our discovery of a very efficient RNAT might explain the previously
776 observed induction of KatY at 37°C in *Y. pestis* [22,23], in particular since the RNAT
777 sequence is entirely conserved between both species (Fig. S5). In contrast to a
778 postulated ROSE (Repression Of heat Shock gene Expression)-like RNAT upstream
779 of *katY* [21], we found a structurally unique regulatory element that reaches almost 25
780 nucleotides into the coding region and is one of the best acting translational silencers
781 in *Y. pseudotuberculosis* identified to date. Concerning the substantial transcriptional
782 upregulation of *katY* (Fig. 2), it is interesting that potential LcrF binding sites have been
783 postulated upstream of *katY* in *Y. pestis* [22,23]. LcrF is the master virulence regulator
784 in *Y. pestis* and *Y. pseudotuberculosis* and itself is subject to stringent temperature
785 control [11,40]. Having KatY production under tight dual temperature control is
786 reminiscent of the situation of the T3SS genes *yopN*, *yscT* and *yscJ*, which are under
787 transcriptional control by LcrF and contain their own RNATs as translational control
788 elements [17,18].

789 The massive induction of KatY at host body temperature as well as its potential
790 association with the membrane or localization in the periplasm [63,64] might suggest
791 a critical role in virulence. At least in *Y. pestis*, however, this is not the case because
792 a *katY* mutant was fully virulent to mice [21] suggesting a certain redundancy in the
793 ROS protection systems. In enterohemorrhagic *E. coli* in contrast it was shown that

794 the secretion of a novel catalase KatN by the T6SS facilitates survival of the pathogen
795 inside macrophages and a deletion of *katN* attenuated virulence [65].

796 Quite obviously, temperature is by far not the only and presumably not the dominant
797 cue inducing the oxidative stress response in bacteria. The paradigmatic system in *E.*
798 *coli* is the H_2O_2-activated transcription factor OxyR [66,67]. Just recently, the influence
799 of H_2O_2 on the expression of ROS detoxification genes in *Y. pseudotuberculosis* was
800 investigated [20]. A total of 364 genes were differentially regulated upon H_2O_2
801 treatment, OxyR was found to be the master transcriptional regulator mediating
802 cellular responses to H_2O_2. Among the upregulated genes were the expected ones
803 responsible for ROS detoxification, like *trxB, trxC, katA, katY* and *ahpC*. The *sodB*
804 gene coding for the iron-containing SOD enzyme was downregulated on the
805 transcriptional level while the other SODs remained unaffected. The authors also
806 investigated the role of KatA/KatE and KatY/KatG in H_2O_2 protection and detoxification
807 at 26°C. Consistent with our findings (Fig. 10), KatA was found to be the primary
808 catalase in *Y. pseudotuberculosis* while KatY, together with AhpR played a strong
809 scavenging activity toward low concentrations of H_2O_2 [20]. Our investigation at two
810 different temperatures added a new role of KatY in ROS protection at 37°C. Massive
811 induction of this catalase at mammalian body temperature might prime the pathogen
812 for the anticipated ROS exposure in the host.

813

814 5 Acknowledgments

815 Funding was provided by the German Research Foundation (DFG NA 240/10-2 and
816 NA 240/14-1 and Research Training Group 2341 “Microbial Substrate Conversion
817 (MiCon)”). We are grateful for support with the catalase assay by Marco Krewing and

Julia Bandow and thank the RNA group for continuous discussions and reading earlier versions of the manuscript.

6 References

1. Jávega B, Herrera G, O'Connor J-E. Flow cytometric analysis of oxidative stress in *Escherichia coli* B strains deficient in genes of the antioxidant defence. International Journal of Molecular Sciences. 2022;23: 6537. doi:10.3390/ijms23126537

2. Imlay JA. Pathways of oxidative damage. Annu Rev Microbiol. 2003;57: 395–418. doi:10.1146/annurev.micro.57.030502.090938

3. Imlay JA. The molecular mechanisms and physiological consequences of oxidative stress: Lessons from a model bacterium. Nat Rev Microbiol. 2013;11: 443–454. doi:10.1038/nrmicro3032

4. Knaus UG, Hertzberger R, Pircalabioru GG, Yousefi SPM, Branco dos Santos F. Pathogen control at the intestinal mucosa – H_2O_2 to the rescue. Gut Microbes. 2017;8: 67–74. doi:10.1080/19490976.2017.1279378

5. Wren BW. The Yersiniae — a model genus to study the rapid evolution of bacterial pathogens. Nat Rev Microbiol. 2003;1: 55–64. doi:10.1038/nrmicro730

6. Farr SB, Kogoma T. Oxidative stress responses in *Escherichia coli* and *Salmonella typhimurium*. Microbiological Reviews. 1991;55: 561–585. doi:10.1128/mr.55.4.561-585.1991

7. Konkel ME, Tilly K. Temperature-regulated expression of bacterial virulence genes. Microbes and Infection. 2000;2: 157–166. doi:10.1016/S1286-4579(00)00272-0

8. Mandin P, Johansson J. Feeling the heat at the millennium: Thermosensors playing with fire. Mol Microbiol. 2020;113: 588–592. doi:10.1111/mmi.14468

9. Steinmann R, Dersch P. Thermosensing to adjust bacterial virulence in a fluctuating environment. Future Microbiol. 2013;8: 85–105. doi:10.2217/fmb.12.129

10. Jackson MW, Silva-Herzog E, Plano GV. The ATP-dependent ClpXP and Lon proteases regulate expression of the *Yersinia pestis* type III secretion system via regulated proteolysis of YmoA, a small histone-like protein. Mol Microbiol. 2004;54: 1364–1378. doi:10.1111/j.1365-2958.2004.04353.x

852 11. Böhme K, Steinmann R, Kortmann J, Seekircher S, Heroven AK, Berger E, et
853 al. Concerted actions of a thermo-labile regulator and a unique intergenic RNA
854 thermosensor control *Yersinia* virulence. PLOS Pathogens. 2012;8: e1002518.
855 doi:10.1371/journal.ppat.1002518

856 12. Schwiesow L, Lam H, Dersch P, Auerbuch V. *Yersinia* type III secretion system
857 master regulator LcrF. J Bacteriol. 2016;198: 604–614. doi:10.1128/JB.00686-15

858

859 13. Nuss AM, Heroven AK, Waldmann B, Reinkensmeier J, Jarek M, Beckstette M,
860 et al. Transcriptomic profiling of *Yersinia pseudotuberculosis* reveals
861 reprogramming of the Crp regulon by temperature and uncovers Crp as a master
862 regulator of small RNAs. PLOS Genetics. 2015;11: e1005087.
863 doi:10.1371/journal.pgen.1005087

864 14. Righetti F, Nuss AM, Twittenhoff C, Beele S, Urban K, Will S, et al.
865 Temperature-responsive *in vitro* RNA structurome of *Yersinia pseudotuberculosis*.
866 Proceedings of the National Academy of Sciences. 2016;113: 7237–7242.
867 doi:10.1073/pnas.1523004113

868 15. Twittenhoff C, Brandenburg VB, Righetti F, Nuss AM, Mosig A, Dersch P, et al.
869 Lead-seq: transcriptome-wide structure probing *in vivo* using lead(II) ions. Nucleic
870 Acids Res. 2020;48: e71. doi:10.1093/nar/gkaa404

871 16. Scheller D, Twittenhoff C, Becker F, Holler M, Narberhaus F. OmpA, a common
872 virulence factor, is under RNA thermometer control in *Yersinia pseudotuberculosis*.
873 Frontiers in Microbiology. 2021;12. doi: 10.3389/fmicb.2021.687260.

874 17. Pienkoß S, Javadi S, Chaoprasid P, Holler M, Roßmanith J, Dersch P, et al.
875 RNA thermometer-coordinated assembly of the *Yersinia* injectisome. Journal of
876 Molecular Biology. 2022;434: 167667. doi:10.1016/j.jmb.2022.167667

877 18. Pienkoß S, Javadi S, Chaoprasid P, Nolte T, Twittenhoff C, Dersch P, et al. The
878 gatekeeper of *Yersinia* type III secretion is under RNA thermometer control. PLOS
879 Pathogens. 2021;17: e1009650. doi:10.1371/journal.ppat.1009650

880 19. Twittenhoff C, Heroven AK, Mühlen S, Dersch P, Narberhaus F. An RNA
881 thermometer dictates production of a secreted bacterial toxin. PLOS Pathogens.
882 2020;16: e1008184. doi:10.1371/journal.ppat.1008184

883 20. Wan F, Feng X, Yin J, Gao H. Distinct H_2O_2-scavenging system in *Yersinia*
884 *pseudotuberculosis*: KatG and AhpC act together to scavenge endogenous
885 hydrogen peroxide. Frontiers in Microbiology. 2021;12. doi:
886 10.3389/fmicb.2021.626874.

887 21. Han Y, Geng J, Qiu Y, Guo Z, Zhou D, Bi Y, et al. Physiological and regulatory
888 characterization of KatA and KatY in *Yersinia pestis*. DNA Cell Biol. 2008;27: 453–
889 462. doi:10.1089/dna.2007.0657

890 22. Garcia E, Nedialkov YA, Elliott J, Motin VL, Brubaker RR. Molecular
891 characterization of KatY (Antigen 5), a thermoregulated chromosomally encoded

892 catalase-peroxidase of *Yersinia pestis*. Journal of Bacteriology. 1999;181: 3114–
893 3122. doi:10.1128/JB.181.10.3114-3122.1999

894 23. Chromy BA, Choi MW, Murphy GA, Gonzales AD, Corzett CH, Chang BC, et
895 al. Proteomic characterization of *Yersinia pestis* virulence. Journal of Bacteriology.
896 2005;187: 8172–8180. doi:10.1128/JB.187.23.8172-8180.2005

897 24. Horton RM, Hunt HD, Ho SN, Pullen JK, Pease LR. Engineering hybrid genes
898 without the use of restriction enzymes: gene splicing by overlap extension. Gene.
899 1989;77: 61–68. doi:10.1016/0378-1119(89)90359-4

900 25. Gaubig LC, Waldminghaus T, Narberhaus F. Multiple layers of control govern
901 expression of the *Escherichia coli ibpAB* heat-shock operon. Microbiology.
902 2011;157: 66–76. doi:10.1099/mic.0.043802-0

903 26. Pfaffl MW. A new mathematical model for relative quantification in real-time RT-
904 PCR. Nucleic Acids Res. 2001;29: e45. doi:10.1093/nar/29.9.e45

905 27. Brantl S, Wagner EG. Antisense RNA-mediated transcriptional attenuation
906 occurs faster than stable antisense/target RNA pairing: An *in vitro* study of plasmid
907 pIP501. EMBO J. 1994;13: 3599–607. doi:10.1046/j.1365-2958.2000.01813.x

908 28. Hartz D, McPheeters DS, Traut R, Gold L. Extension inhibition analysis of
909 translation initiation complexes. Methods in Enzymology. Academic Press; 1988.
910 pp. 419–425. doi:10.1016/S0076-6879(88)64058-4

911 29. Degrossoli A, Müller A, Xie K, Schneider JF, Bader V, Winklhofer KF, et al.
912 Neutrophil-generated HOCl leads to non-specific thiol oxidation in phagocytized
913 bacteria. Winterbourn C, editor. eLife. 2018;7: e32288. doi:10.7554/eLife.32288

914 30. Reuter WH, Masuch T, Ke N, Lenon M, Radzinski M, Van Loi V, et al. Utilizing
915 redox-sensitive GFP fusions to detect *in vivo* redox changes in a genetically
916 engineered prokaryote. Redox Biology. 2019;26: 101280.
917 doi:10.1016/j.redox.2019.101280

918 31. Aebi H. Catalase *in vitro*. Methods in Enzymology. Academic Press; 1984. pp.
919 121–126. doi:10.1016/S0076-6879(84)05016-3

920 32. Hanson GT, Aggeler R, Oglesbee D, Cannon M, Capaldi RA, Tsien RY, et al.
921 Investigating mitochondrial redox potential with redox-sensitive green fluorescent
922 protein indicators. Journal of Biological Chemistry. 2004;279: 13044–13053.
923 doi:10.1074/jbc.M312846200

924 33. Gutscher M, Sobotta MC, Wabnitz GH, Ballikaya S, Meyer AJ, Samstag Y, et
925 al. Proximity-based protein thiol oxidation by H_2O_2-scavenging peroxidases.
926 Journal of Biological Chemistry. 2009;284: 31532–31540.
927 doi:10.1074/jbc.M109.059246

928 34. Nickerson CA, Achberger EC. Role of curved DNA in binding of *Escherichia*
929 *coli* RNA polymerase to promoters. J Bacteriol. 1995;177: 5756–5761.

930 35. Tupper AE, Owen-Hughes TA, Ussery DW, Santos DS, Ferguson DJ,
931 Sidebotham JM, et al. The chromatin-associated protein H-NS alters DNA topology
932 *in vitro*. EMBO J. 1994;13: 258–268. doi:10.1002/j.1460-2075.1994.tb06256.x

933 36. Balderas D, Ohanyan M, Alvarez PA, Mettert E, Tanner N, Kiley PJ, et al.
934 Repression by the H-NS/YmoA histone-like protein complex enables IscR
935 dependent regulation of the *Yersinia* T3SS. PLOS Genetics. 2022;18: e1010321.
936 doi:10.1371/journal.pgen.1010321

937

938 37. Böhme K, Heroven AK, Lobedann S, Guo Y, Stolle A-S, Dersch P. The small
939 protein YmoA controls the Csr system and adjusts expression of virulence-relevant
940 traits of *Yersinia pseudotuberculosis*. Front Microbiol. 2021;12: 706934.
941 doi:10.3389/fmicb.2021.706934

942 38. Grosso-Becera MV, Servín-González L, Soberón-Chávez G. RNA structures
943 are involved in the thermoregulation of bacterial virulence-associated traits. Trends
944 Microbiol. 2015;23: 509–518. doi:10.1016/j.tim.2015.04.004

945 39. Loh E, Righetti F, Eichner H, Twittenhoff C, Narberhaus F. RNA thermometers
946 in bacterial pathogens. Microbiol Spectr. 2018;6. doi:10.1128/microbiolspec.RWR-
947 0012-2017

948 40. Hoe NP, Goguen JD. Temperature sensing in *Yersinia pestis*: Translation of
949 the LcrF activator protein is thermally regulated. J Bacteriol. 1993;175: 7901–7909.
950 doi:10.1128/jb.175.24.7901-7909.1993

951 41. Johansson J, Mandin P, Renzoni A, Chiaruttini C, Springer M, Cossart P. An
952 RNA thermosensor controls expression of virulence genes in *Listeria*
953 *monocytogenes*. Cell. 2002;110: 551–561. doi:10.1016/s0092-8674(02)00905-4

954 42. Weber GG, Kortmann J, Narberhaus F, Klose KE. RNA thermometer controls
955 temperature-dependent virulence factor expression in *Vibrio cholerae*. Proc Natl
956 Acad Sci U S A. 2014;111: 14241–14246. doi:10.1073/pnas.1411570111

957 43. Wei Y, Kouse AB, Murphy ER. Transcriptional and posttranscriptional
958 regulation of *Shigella shuT* in response to host-associated iron availability and
959 temperature. Microbiologyopen. 2017;6: e00442. doi:10.1002/mbo3.442

960 44. Brewer SM, Twittenhoff C, Kortmann J, Brubaker SW, Honeycutt J, Massis LM,
961 et al. A *Salmonella Typhi* RNA thermosensor regulates virulence factors and innate
962 immune evasion in response to host temperature. PLoS Pathog. 2021;17:
963 e1009345. doi:10.1371/journal.ppat.1009345

964 45. Fang FC. Antimicrobial reactive oxygen and nitrogen species: concepts and
965 controversies. Nat Rev Microbiol. 2004;2: 820–832. doi:10.1038/nrmicro1004

966 46. Holmgren A. Thioredoxin. Annu Rev Biochem. 1985;54: 237–271.
967 doi:10.1146/annurev.bi.54.070185.001321

968 47. Masip L, Veeravalli K, Georgiou G. The many faces of glutathione in bacteria.
969 Antioxid Redox Signal. 2006;8: 753–762. doi:10.1089/ars.2006.8.753

970 48. Brouwer S, Pustelny C, Ritter C, Klinkert B, Narberhaus F, Häussler S. The
971 PqsR and RhlR transcriptional regulators determine the level of *Pseudomonas*
972 quinolone signal synthesis in *Pseudomonas aeruginosa* by producing two different
973 *pqsABCDE* mRNA isoforms. J Bacteriol. 2014;196: 4163–4171.
974 doi:10.1128/JB.02000-14

975

976 49. Rosso M-L, Chauvaux S, Dessein R, Laurans C, Frangeul L, Lacroix C, et al.
977 Growth of *Yersinia pseudotuberculosis* in human plasma: Impacts on virulence and
978 metabolic gene expression. BMC Microbiol. 2008;8: 211. doi:10.1186/1471-2180-
979 8-211

980 50. Roggenkamp A, Bittner T, Leitritz L, Sing A, Heesemann J. Contribution of the
981 Mn-cofactored superoxide dismutase (SodA) to the virulence of *Yersinia*
982 *enterocolitica* serotype O8. Infect Immun. 1997;65: 4705–4710.
983 doi:10.1128/iai.65.11.4705-4710.1997

984 51. Champion OL, Cooper IAM, James SL, Ford D, Karlyshev A, Wren BW, et al.
985 *Galleria mellonella* as an alternative infection model for *Yersinia*
986 *pseudotuberculosis*. Microbiology. 2009;155: 1516–1522.
987 doi:10.1099/mic.0.026823-0

988 52. Chareyre S, Mandin P. Bacterial iron homeostasis regulation by sRNAs.
989 Microbiol Spectr. 2018;6. doi:10.1128/microbiolspec.RWR-0010-2017

990 53. Afonyushkin T, Večerek B, Moll I, Bläsi U, Kaberdin VR. Both RNase E and
991 RNase III control the stability of *sodB* mRNA upon translational inhibition by the
992 small regulatory RNA RyhB. Nucleic Acids Res. 2005;33: 1678–1689.
993 doi:10.1093/nar/gki313

994 54. Prévost K, Desnoyers G, Jacques J-F, Lavoie F, Massé E. Small RNA-induced
995 mRNA degradation achieved through both translation block and activated
996 cleavage. Genes Dev. 2011;25: 385–396. doi:10.1101/gad.2001711

997 55. Massé E, Gottesman S. A small RNA regulates the expression of genes
998 involved in iron metabolism in *Escherichia coli*. Proc Natl Acad Sci U S A. 2002;99:
999 4620–4625. doi:10.1073/pnas.032066599

1000 56. Imlay JA, Chin SM, Linn S. Toxic DNA damage by hydrogen peroxide through
1001 the Fenton reaction *in vivo* and *in vitro*. Science. 1988;240: 640–642.
1002 doi:10.1126/science.2834821

1003 57. Chauvaux S, Rosso M-L, Frangeul L, Lacroix C, Labarre L, Schiavo A, et al.
1004 Transcriptome analysis of *Yersinia pestis* in human plasma: An approach for
1005 discovering bacterial genes involved in septicaemic plague. Microbiology.
1006 2007;153: 3112–3124. doi:10.1099/mic.0.2007/006213-0

58. Wang T, Si M, Song Y, Zhu W, Gao F, Wang Y, et al. Type VI secretion system transports Zn^{2+} to combat multiple stresses and host immunity. PLoS Pathog. 2015;11: e1005020. doi:10.1371/journal.ppat.1005020

59. Wang T, Yang X, Gao F, Zhao C, Kang Y, Wang Y, et al. Zinc acquisition via ZnuABC in *Yersinia pseudotuberculosis* facilitates resistance to oxidative stress. Ann Microbiol. 2016;66: 1189–1197. doi:10.1007/s13213-016-1205-7

60. Rinnenthal J, Klinkert B, Narberhaus F, Schwalbe H. Modulation of the stability of the *Salmonella* fourU-type RNA thermometer. Nucleic Acids Res. 2011;39: 8258–8270. doi:10.1093/nar/gkr314

61. Gao M, Gnutt D, Orban A, Appel B, Righetti F, Winter R, et al. RNA hairpin folding in the crowded cell. Angew Chem Int Ed Engl. 2016;55: 3224–3228. doi:10.1002/anie.201510847

62. Yoo H, Davis CM. An *in vitro* cytomimetic of in-cell RNA folding. Chembiochem. 2022;23: e202200406. doi:10.1002/cbic.202200406

63. Myers-Morales T, Cowan C, Gray ME, Wulff CR, Parker CE, Borchers CH, et al. A surface-focused biotinylation procedure identifies the *Yersinia pestis* catalase KatY as a membrane-associated but non-surface-located protein. Applied and Environmental Microbiology. 2007;73: 5750–5759. doi:10.1128/AEM.02968-06

64. Smither SJ, Hill J, van Baar BLM, Hulst AG, de Jong AL, Titball RW. Identification of outer membrane proteins of *Yersinia pestis* through biotinylation. Journal of Microbiological Methods. 2007;68: 26–31. doi:10.1016/j.mimet.2006.05.014

65. Wan B, Zhang Q, Ni J, Li S, Wen D, Li J, et al. Type VI secretion system contributes to Enterohemorrhagic *Escherichia coli* virulence by secreting catalase against host reactive oxygen species (ROS). PLoS Pathog. 2017;13: e1006246. doi:10.1371/journal.ppat.1006246

66. Imlay JA. Transcription factors that defend bacteria against reactive oxygen species. Annu Rev Microbiol. 2015;69: 93–108. doi:10.1146/annurev-micro-091014-104322

67. Sen A, Imlay JA. How microbes defend themselves from incoming hydrogen peroxide. Front Immunol. 2021;12: 667343. doi:10.3389/fimmu.2021.667343

D1. Supplementary information

The oxidative stress response, in particular the *katY* gene, is temperature-regulated in *Yersinia pseudotuberculosis*

Daniel Scheller[1], Franziska Becker[1], Andrea Wimbert[1], Dominik Meggers[1], Stephan Pienkoß[1], Christian Twittenhoff[1], Lisa Knoke[2], Lars Leichert[2], Franz Narberhaus[1*]

[1]Ruhr University Bochum, Faculty of Biology and Biotechnology, Microbial Biology, 44780 Bochum, Germany

[2]Ruhr University Bochum, Faculty of Medicine, Institute of Biochemistry and Pathobiochemistry, Microbial Biochemistry, 44780 Bochum, Germany

Short title: *Yersinia* oxidative stress response regulation

*** Corresponding author:** franz.narberhaus@rub.de

Supplementary information:

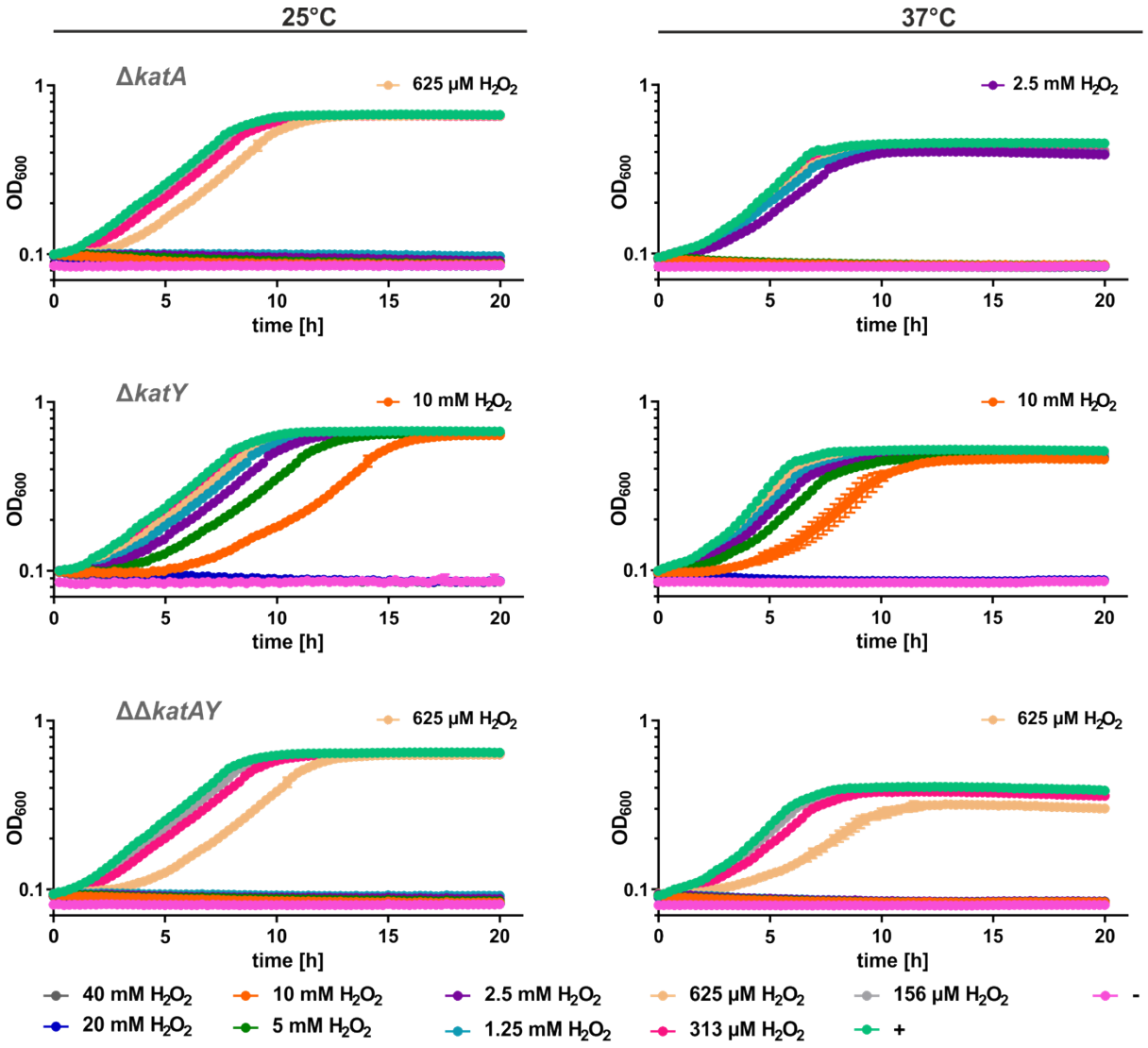

Fig S1. Deletion of *katA* and *katY* affect susceptibility against H_2O_2. Cells were pre-grown at 25°C or 37°C and diluted to an OD_{600} of 0.05 in a 96 well plate. H_2O_2 was added to the indicated final concentrations. Growth was monitored by reading the OD_{600} during incubation at 25°C or 37°C. The highest concentration, which allowed growth is highlighted. + = no H_2O_2 control, - = medium control. The mean and the standard deviation of biological triplicates are plotted.

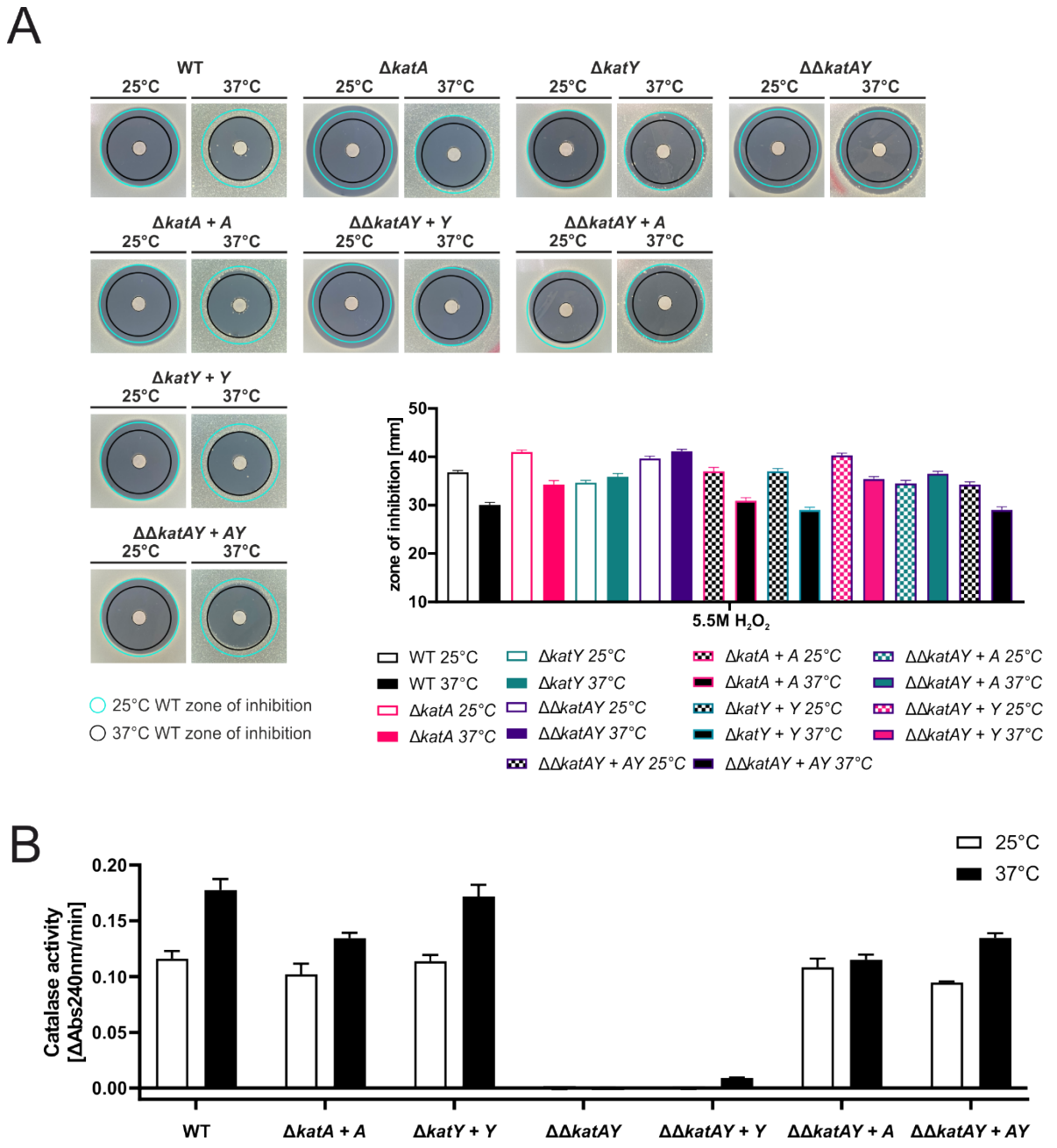

Fig S2. Temperature-dependent influence of *katA* and *katY* on the oxidative stress response is restored by complementation in *Y. pseudotuberculosis*. (A) Disk diffusion assay for H_2O_2 was conducted by applying 3 µl of 5.5 M H_2O_2 onto paper disks on soft agar containing a bacterial suspension. After 24 h of growth at the indicated temperature the zone of inhibition was measured. Results from one representative experiment are shown. The experiment was carried out multiple times and each time in biological triplicates and two technical replicates. Cyan ring = zone of inhibition measured for the wildtype at 25°C. Black ring = zone of inhibition measured for the wildtype at 37°C. **(B)** Decomposition of H_2O_2 was measured in real-time by reading the absorption of H_2O_2 at 240 nm over time at 25°C. Cells were grown at 25°C or 37°C until an OD_{600} of 0.5 was reached. Cells were lysed by ultrasonication. Lysate with a protein concentration of 50 µg/ml, determined by Bradford assay, was used and treated with 0.01 M H_2O_2. The velocity of H_2O_2 decomposition was calculated based on the linear range at the beginning of the curve. Experiments were carried out at least twice in biological triplicates.

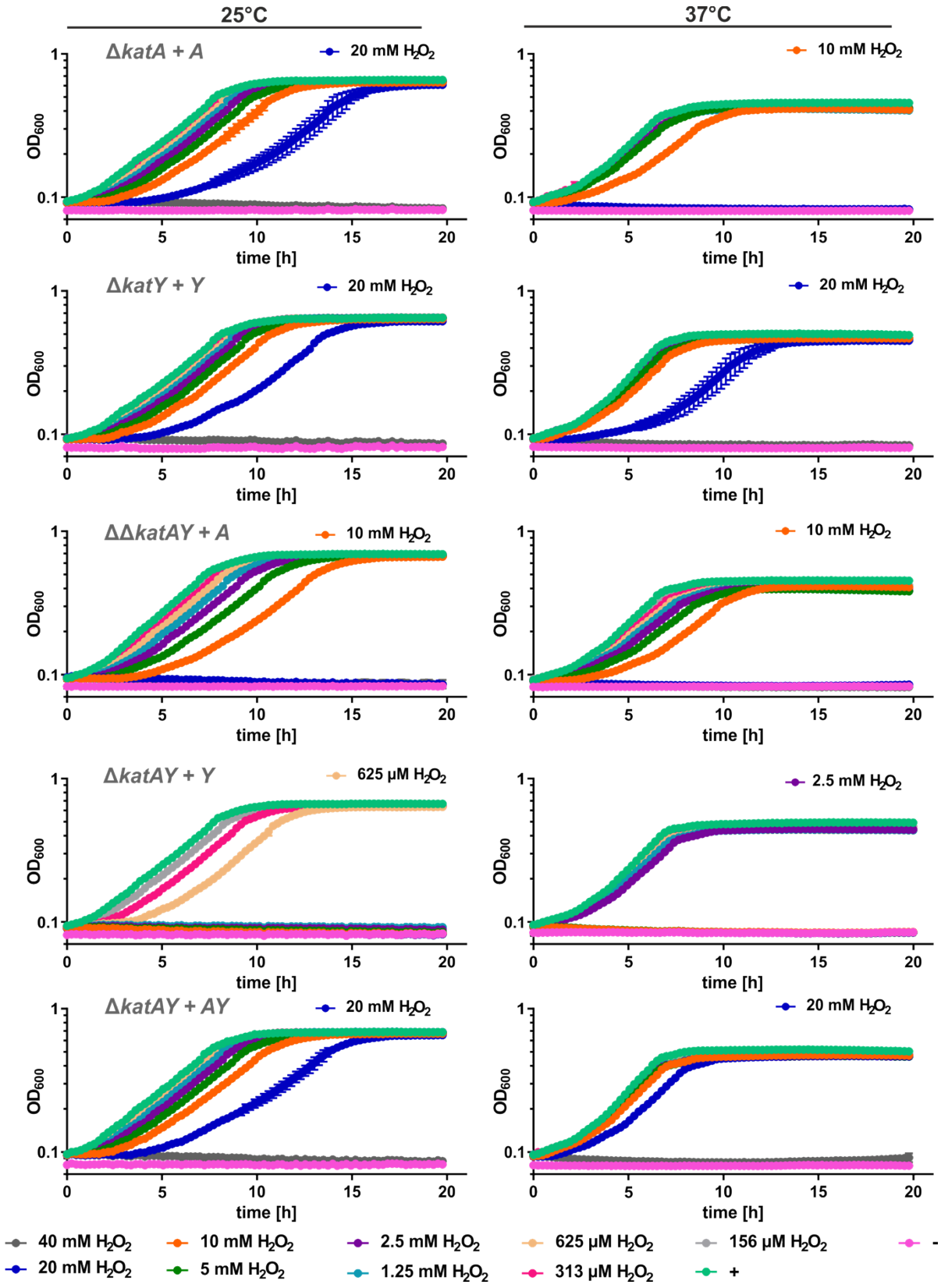

Fig S3. Temperature-dependent influence of *katA* and *katY* on the oxidative stress response during growth is restored by complementation in *Y. pseudotuberculosis*. Cells were pre-grown at 25°C or 37°C and diluted to an OD_{600} of 0.05 in a 96 well plate. H_2O_2 was added to the indicated final concentrations. Growth was monitored by measuring the OD_{600}

during incubation at 25°C or 37°C. The highest concentration, which allowed growth is highlighted. + = no H_2O_2 control, - = medium control. The mean and the standard deviation of biological triplicates are plotted. Experiments were carried out multiple times.

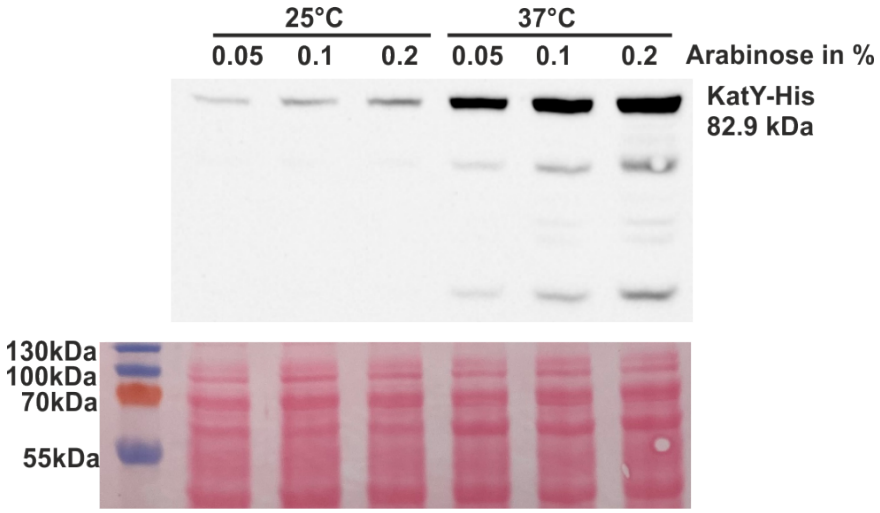

Figure S4. **The *katY* RNAT controls translation in a plasmid-based complementation**. The *katY* deletion strain was complemented with a plasmid containing arabinose-inducible KatY with a C-terminal His tag. Cells were grown to an OD_{600} of 0.5 at 25 and 37°C. Subsequently, transcription was induced by the addition of L-arabinose. After 30 min of incubation, samples were taken for Western blot analysis. Western blot membranes were stained with Ponceau S as a loading control. One representative Western blot is shown.

```
                                                    SD
Y. pestis KIM10          TAATCATGTTAAAAAATAGTTGCCTTTTAGTTAAAGGGGACTTATATATGTTAAAAAAAATCTTACCCGTACTAATA
Y. pseudotuberculosis YPIII                GCCTTTTAGTTAAAGGGGACTTATATATGTTAAAAAAAATCTTACCCGTACTAATA
                           **********************************************************
```

Figure S5. **Sequence alignment of the upstream region of *katY* between *Y. pestis* and *Y. pseudotuberculosis*.** Sequence comparision of the RNA thermometer sequence of *katY* of *Y. pseudotuberculosis* against the upstream region of *katY* of *Y. pestis*. The putative SD region and the start codon (blue) are indicated.

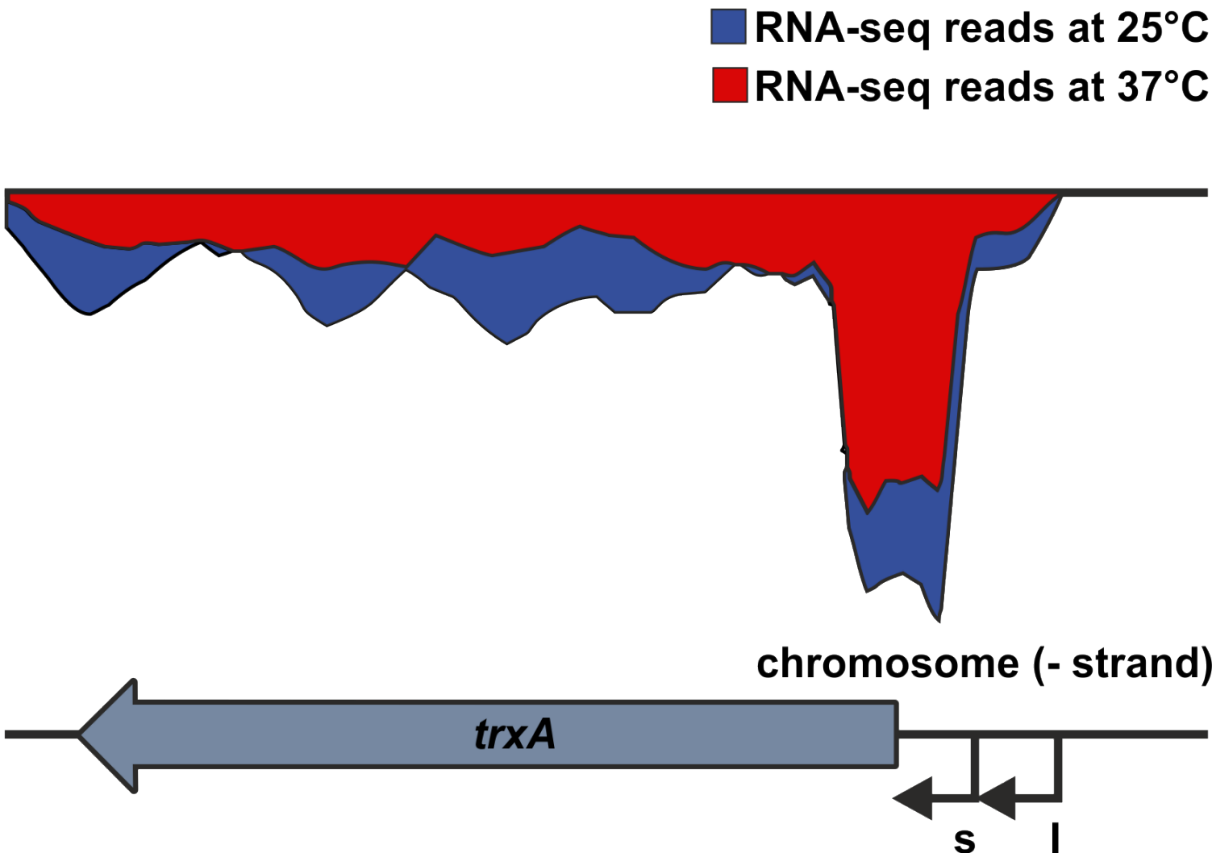

Figure S6. **The short *trxA* transcript is the more abundant isoform.** RNA-seq results of the *trxA* transcript at 25 and 37°C and identification of two transcriptional start sites by [1]. s = start site of the short transcript, l = start site of the long transcript.

Table S1: RNA-seq results 37/25°C

			accession ID	NC_010465.1			mean read counts				
locus	**old locus**	**strand**	**start**	**stop**	**gene**	**gene discription**	**YPIII_E25**	**YPIII_E37**	**log2 Fold change**	**p-value**	**padjust**
YPK_RS00160	YPK_0035	-	38131	38754	***sodA***	superoxide dismutase [Mn]	1678.2	1344.0	**-0.32**	0.000	0.001
YPK_RS09375	YPK_1863	-	2070933	2071511	***sodB***	superoxide dismutase [Fe]	326.1	667.8	**1.03**	0.000	0.000
YPK_RS14285	YPK_2855	+	3147393	3148832	***katA***	catalase	43.7	347.8	**2.99**	0.000	0.000
YPK_RS16370	YPK_3267	+	3571791	3572393	***ahpC***	alkyl hydroperoxide reductase	1484.6	1811.2	**0.29**	0.002	0.005
YPK_RS17025	YPK_3388	+	3717303	3719516	***katY***	catalase/peroxidase HPI	71.8	2149.6	**4.90**	0.000	0.000
YPK_RS17310	YPK_3445	-	3778490	3779095	***sodC***	superoxide dismutase	1385.1	4452.0	**1.63**	0.000	0.000
YPK_RS20330	YPK_4035	-	4451596	4451922	***trxA***	thioredoxin TrxA	2189.9	1849.7	**-0.24**	0.010	0.020
YPK_RS20895	YPK_4139	-	4571109	4571357	***grxC***	glutaredoxin 3	1330.3	732.1	**-0.86**	0.000	0.000

Table S2: Bacterial strains

Strain	**Relevant characteristics**	**Reference**
Yersinia pseudotuberculosis		
YPIII	pIB1, wild type	[2]
YPIII Δ*katA*	pIB1 Δ*katA*	This study
YPIII Δ*katY*	pIB1 Δ*katY*	This study
YPIII ΔΔ*katAY*	pIB1 ΔΔ*katAY*	This study
YPIII Δ*katA* + *katA*-His	pIB1 Δ*katA;* reintroduction of His-tagged KatA by homologous recombination	This study
YPIII Δ*katY* + *katY*-His	pIB1 Δ*katY;* reintroduction of His-tagged KatY by homologous recombination	This study
YPIII ΔΔ*katAY* + *katA*-His	pIB1 ΔΔ*katAY;* reintroduction of His-tagged KatA by homologous recombination	This study
YPIII ΔΔ*katAY* + *katY*-His	pIB1 ΔΔ*katAY;* reintroduction of His-tagged KatY by homologous recombination	This study
YPIII ΔΔ*katAY* + *katA*-His and *katY*-His	pIB1 ΔΔ*katAY* + *katA*-His*;* reintroduction of His-tagged KatY by homologous recombination	This study
Escherichia coli		
DH5α	*supE44*, Δ*lacU169* (ψ80*lacZ*Δ*M15*), *hsdR17*, *recA1*, *gyrA96*, *thi1*, *relA1*	[3]
S17-1 *λpir*	*RP4-2 Tc::Mu-Km::Tn7 (λpir)*	[4]

Table S3: Plasmid list

Plasmid	Relevant characteristics	Reference
pUC18	Cloning vector; Ap^r	[5]
pDM4	*sacBR, oriT, oriR6K,* Cm^r	[6]
pCC_roGFP2-orp1	Redox sensitive probe*, roGFP2-orp1; ptac*	[7]
pBAD2-*bgaB*-His	*bgaB* reporter gene vector, Ap^r, araC, P_{BAD} promoter, His-Tag at the C-terminal end of BgaB	[8]
pBAD-His A	Expression vector, Ap^r, araC, P_{BAD} promoter, N-terminal His-Tag	Invitrogen, Carlsbad, CA
pBO6202	pBAD2-bgaB-His, short 5'-UTR of *yopN* (pYP0065) plus 30 bp of the coding region, (-37 to +30 bp from *yopN* ATG)	[9]
pBO4423	pBAD2-bgaB-His; 5'-UTR of *sodA* (YPK_0035) plus 30 bp of *sodA* coding region (-55 to +30 bp from *sodA* ATG)	[8]
pBO4406	pBAD2-bgaB-His; 5'-UTR of *sodB* (YPK_1863) plus 30 bp of *sodB* coding region (-89 to +30 bp from *sodB* ATG)	[8]
pBO4902	pBAD2-bgaB-His; 5'-UTR of *sodB* (YPK_1863) plus 30 bp of *sodB* coding region (-89 to +30 bp from *sodB* ATG), mutant Rep AA70-71CT,C73T	This study
pBO4914	pUC18; YPK_1863 (*sodB*) 5'-UTR plus coding region (-89 to +60 bp from *sodB* ATG); runoff plasmid for structure probing and primer extension inhibition	This study
pBO4917	pUC18; YPK_1863 (*sodB*) 5'-UTR plus coding region (-89 to +60 bp from *sodB* ATG), mutant Rep AA70-71CT,C73T; runoff plasmid for structure probing and primer extension inhibition	This study
pBO4909	pBAD2-bgaB-His; 5'-UTR of *sodC* (YPK_3445) plus 30 bp of *sodC* coding region (-63 to +30 bp from *sodC* ATG)	This study
pBO6861	pBAD2-bgaB-His; 5'-UTR of *sodC* (YPK_3445) plus 30 bp of *sodC* coding region (-63 to +30 bp from *sodC* ATG) mutant Rep TG83-84CC	This study
pBO4916	pUC18; YPK_3445 (*sodC*) 5'-UTR plus coding region (-63 to +60 bp from *sodC* ATG); runoff plasmid for structure probing and primer extension inhibition	This study

pBO6864	pUC18; YPK_3445 (*sodC*) 5'-UTR plus coding region (-63 to +60 bp from *sodC* ATG), mutant Rep TG83-84CC; runoff plasmid for structure probing and primer extension inhibition	This study
pBO4416	pBAD2-bgaB-His; 5'-UTR of *katA* (YPK_2855) plus 30 bp of *katA* coding region (-121 to +30 bp from katA ATG)	[8]
pBO4905	pBAD2-bgaB-His; 5'-UTR of *katA* (YPK_2855) plus 30 bp of *katA* coding region (-121 to +30 bp from katA ATG) Mutant Rep AC109-110CG	This study
pBO4915	pUC18; YPK_2855 (*katA*) 5'-UTR plus coding region (-121 to +60 bp from *katA* ATG); runoff plasmid for structure probing and primer extension inhibition	This study
pBO4918	pUC18; YPK_2855 (*katA*) 5'-UTR plus coding region (-121 to +60 bp from *katA* ATG), mutant Rep AC109-110CG; runoff plasmid for structure probing and primer extension inhibition	This study
pBO4436	pBAD2-bgaB-His; 5'-UTR of *katY* (YPK_3388) plus 30 bp of *katY* coding region (-26 to +30 bp from *katY* ATG)	This study
pBO6887	pBAD2-bgaB-His; 5'-UTR of *katY* (YPK_3388) plus 30 bp of *katY* coding region (-26 to +30 bp from *katY* ATG) mutant Rep T31C	This study
pBO6886	pBAD2-bgaB-His; 5'-UTR of *katY* (YPK_3388) plus 30 bp of *katY* coding region (-26 to +30 bp from *katY* ATG) mutant Derep TA31-32CT	This study
pBO7248	pUC18; YPK_3388 (*katY*) 5'-UTR plus coding region (-26 to +30 bp from *katA* ATG); runoff plasmid for structure probing	This study
pBO7238	pUC18; YPK_3388 (*katY*) 5'-UTR plus coding region (-26 to +60 bp from *katA* ATG); runoff plasmid for primer extension inhibition	This study
pBO3179	pBAD2-bgaB-His; short 5'-UTR of *trxA* (YPK_4035) plus 30 bp of *trxA* coding region (-58 to +30 bp from *trxA* ATG)	[8]
pBO6859	pBAD2-bgaB-His; short 5'-UTR of *trxA* (YPK_4035) plus 30 bp of *trxA* coding region (-58 to +30 bp from *trxA* ATG) Mutant Rep A24T	This study
pBO3178	pBAD2-bgaB-His; long 5'-UTR of *trxA* (YPK_4035) plus 30 bp of *trxA* coding region (-98 to +30 bp from *trxA* ATG)	[8]
pBO6862	pBAD2-bgaB-His; long 5'-UTR of *trxA* (YPK_4035) plus 30 bp of *trxA* coding region (-98 to +30 bp from *trxA* ATG) Mutant Rep A79C	This study
pBO6857	pUC18; short YPK_4035 (*trxA*) 5'-UTR plus coding region (-58 to +60 bp from *trxA* ATG); runoff plasmid for structure probing and primer extension inhibition	This study

pBO6858	pUC18; short YPK_4035 (*trxA*) 5'-UTR plus coding region (-58 to +60 bp from *trxA* ATG), mutant Rep A24T; runoff plasmid for structure probing and primer extension inhibition	This study
pBO6863	pUC18; long YPK_4035 (*trxA*) 5'-UTR plus coding region (-98 to +60 bp from *trxA* ATG); runoff plasmid for structure probing and primer extension inhibition	This study
pBO7246	pBAD-His A Expression vector, 5'-UTR and *katY* (YPK_3388) with a His-tag at the C-terminal end	This study
pBO6868	pDM4, *katA* deletion fragment for generation of Δ*katA* by bacterial conjugation	This study
pBO7212	pDM4, *katY* deletion fragment for generation of Δ*katY* by bacterial conjugation	This study
pBO6888	pDM4, *katA*-His complementation fragment for restoration of *katA* with a C-terminal His-tag by bacterial conjugation	This study
pBO7251	pDM4, *katY*-His complementation fragment for restoration of *katY* with a C-terminal His-tag by bacterial conjugation	This study

Table S4: Oligonucleotide list

Name	Purpose	Plasmid	Sequence (5'->3')
sodB_ro_fw	forward primer to amplify YPK_1863 (*sodB*) 5'-UTR with a T7 promoter for the construction of the runoff plasmid	pBO4914	AGAAATTAATACGACTCACT ATAGGGTTTTAACCGCTCTT CACCC
sodB_ro_rev	reverse primer to amplify YPK_1863 (*sodB*) 5'-UTR + 60 bp from ATG; reverse primer with NaeI site for the construction of the runoff plasmid for structure probing and primer extension inhibition	pBO4914	GCCGGCAGAGATGTGGGGT TCCAG
sodB_rep_fw	mutagenesis forward primer to introduce the mutation AA70-71CT, C73T into YPK_1863 (*sodB*) 5'-UTR	pBO4902 pBO4917	GAGCAAACACCCTGAGCCTC TCCGAAAGGAGAGAGCT
sodB_rep_rev	mutagenesis reverse primer to introduce the mutation AA70-71CT, C73T into YPK_1863 (*sodB*) 5'-UTR	pBO4902 pBO4917	AGCTCTCTCCTTTCGGAGAG GCTCAGGGTGTTTGCTC

sodC_UTR_fw	forward primer to amplify the 5'-UTR of YPK_3445 (*sodC*) plus 30 bp of *sodC* coding region (-63 to +30 bp from *sodC* ATG)	pBO4909	TTGCTAGCGTCAAAAGTTTC CTATTGACAA
sodC_UTR_rev	reverse primer to amplify the 5'-UTR of YPK_3445 (*sodC*) plus 30 bp of *sodC* coding region (-63 to +30 bp from *sodC*	pBO4909	TTGAATTCAACAGGTAGCAA TAATGTAATT
sodC_ro_fw	forward primer to amplify YPK_3445 (*sodC*) 5'-UTR with a T7 promoter for the construction of the runoff plasmid	pBO4916	AGAAATTAATACGACTCACT ATAGGGGTCAAAAGTTTCCT ATTGACAA
sodC_ro_rev	reverse primer to amplify YPK_3445 (*sodC*) 5'-UTR + 60 bp from ATG; reverse primer with NaeI site for the construction of the runoff plasmid for structure probing and primer extension inhibition	pBO4916	GCCGGCAGCGGCCAGTGTTG CG
sodC_rep_fw	mutagenesis forward primer to introduce the mutation TG83-84CC into YPK_3445 (*sodC*) 5'-UTR	pBO6861 pBO6864	TGAAATTAATTACATTATCC CTACCTGTTATTCTTTAC
sodC_rep_rev	mutagenesis reverse primer to introduce the mutation TG83-84CC into YPK_3445 (*sodC*) 5'-UTR	pBO6861 pBO6864	GTAAAGAATAACAGGTAGG GATAATGTAATTAATTTCA
katA_ro_fw	forward primer to amplify YPK_2855 (*katA*) 5'-UTR with a T7 promoter for the construction of the runoff plasmid	pBO4915	AGAAATTAATACGACTCACT ATAGGGGAGATCAAAGAAT AACACCGT
katA_ro_rev	reverse primer to amplify YPK_2855 (*katA*) 5'-UTR + 60 bp from ATG; reverse primer with NaeI site for the construction of the runoff plasmid for structure probing and primer extension inhibition	pBO4915	GCCGGCATTATTATTATCGA CAACGGG
katA_rep_fw	mutagenesis forward primer to introduce the mutation AC109-110CG into YPK_2855 (*katA*) 5'-UTR	pBO4905 pBO4918	CAATCAATTCAACAGCCATC GTGGAGAACATGATGAG
katA_rep_rev	mutagenesis reverse primer to introduce the mutation AC109-110CG into YPK_2855 (*katA)* 5'-UTR	pBO4905 pBO4918	CTCATCATGTTCTCCACGAT GGCTGTTGAATTGATTG

katA_5‘-flank_fw	forward primer to amplify the upstream region (683 bp) of YPK_2855 (*katA)* for deletion of *katA*	pBO6868	TTTGTCGACTTGATCGGATAGCTTAGCCC
katA_5‘-flank rev	reverse primer to amplify the upstream region (683 bp) of YPK_2855 (*katA)* with an overlap to the downstream region (403 bp) of *katA* for deletion of *katA*	pBO6868	TTCAAAGGGGCTGATCGGGTCATGTTCTCCAGTATGGCTG
katA_3’flank_fw	forward primer to amplify the downstream region (403 bp) of YPK_2855 (*katA)* with an overlap to the upstream region (683 bp) for deletion of *katA*	pBO6868	CAGCCATACTGGAGAACATGACCCGATCAGCCCCTTTGAA
katA_3’flank_rev	reverse primer to amplify the upstream region (403 bp) of YPK_2855 (*katA)* for deletion of *katA*	pBO6868	TTTTCTAGATCACTGAGGGAGAGTGGTTA
katA_EP_fw	forward primer to check for deletion/complementation of YPK_2855 (*katA)*	-	AATACGTTCCAACGCACCCC
katA_EP_rev	reverse primer to check for deletion/complementation of YPK_2855 (*katA)*	-	TTATCGGCTAGTCGAAGAGC
katA_IP_fw	forward primer to check for deletion/complementation of YPK_2855 (*katA)*	-	ACGTGATCCACTGAAGTTCC
katA_IP_rev	reverse primer to check for deletion/complementation of YPK_2855 (*katA)*	-	CTTACCGTCATATGCACGG
katA-His_fw	forward primer to amplify the 5’-UTR of YPK_2855 (*katA)* plus *katA* with a His-tag for complementation of Δ*katA*	pBO6888	TTTCCATGGGAGATCAAAGAATAACACCGTG
katA-His_rev	reverse primer to amplify the 5’-UTR of YPK_2855 (*katA)* plus *katA* with a His-tag for complementation of Δ*katA*	pBO6888	TTTTTAGTGGTGATGGTGATGATGATTCAGGCCAAGTGCTTTTTTCA
pDM4_katA_Del_fw	forward primer to linearize the pDM4-*katA*-deletion plasmid for NEB Hifi Assembly	pBO6888	CATGTTCTCCAGTATGGCTG

pDM4_katA_Del_rev	reverse primer to linearize the pDM4-*katA*-deletion plasmid for NEB Hifi Assembly	pBO6888	ACCCGATCAGCCCCTTTG
katA_pDM4_Del_fw	forward primer to amplify the 5'-UTR of YPK_2855 (*katA)* plus *katA* with a His-tag and an overlap to the pDM4-*katA*-deletion plasmid for complementation of Δ*katA*	pBO6888	TTCAAAGGGGCTGATCGGGT TTAGTGGTGATGGTGATG
katA_pDM4_Del_rev	reverse primer to amplify the 5'-UTR of YPK_2855 (*katA)* plus *katA* with a His-tag and an overlap to the pDM4-*katA*-deletion plasmid for complementation of Δ*katA*	pBO6888	CAGCCATACTGGAGAACAT GATGAGCAAGAAGAAAGGA TTAAC
katY_UTR_fw	forward primer to amplify the 5'-UTR of YPK_3388 (*katY*) plus 30 bp of *katY* coding region (-26 to +30 bp from *katY* ATG)	pBO4436	TTGCTAGCGCCTTTTAGTTA AAGGGGAC
katY_UTR_rev	reverse primer to amplify the 5'-UTR of YPK_3388 (*katY*) plus 30 bp of *katY* coding region (-26 to +30 bp from *katY* ATG	pBO4436	TTGAATTCTATTAGTACGGG TAAGATTTTTTT
katY_ro_fw	forward primer to amplify YPK_3388 (*katY*) 5'-UTR with a T7 promoter for the construction of the runoff plasmids	pBO7238 pBO7248	AGAAATTAATACGACTCACT ATAGGGGCTAGCGCCTTTTA GTTAAAGG
katY_ro_30nt_rev	reverse primer to amplify YPK_3388 (*katY*) 5'-UTR + 30 bp from ATG; reverse primer with EcoRV site for the construction of the runoff plasmid for structure probing and primer extension inhibition	pBO7248	AAGATATCTATTAGTACGGG TAAGATTTTTT
katY_ro_rev	reverse primer to amplify YPK_3388 (*katY*) 5'-UTR + 60 bp from ATG; reverse primer with EcoRV site for the construction of the runoff plasmid for structure probing and primer extension inhibition	pBO7238	AAGATATCCGTAGGTGTATT ATGTACAATGGC
katY_rep_fw	mutagenesis forward primer to introduce the mutation T31C into YPK_3388 (*katY*) 5'-UTR	pBO6887	AAGGGGACTTATATATGTCA AAAAAAATCTTACCCGT
katY_rep_rev	mutagenesis reverse primer to introduce the mutation T31C into YPK_3388 (*katY*) 5'-UTR	pBO6887	ACGGGTAAGATTTTTTTGA CATATATAAGTCCCCTT

katY_derep_fw	mutagenesis forward primer to introduce the mutation TA31-32CT into YPK_3388 (*katY*) 5‘-UTR	pBO6886	AAGGGGACTTATATATGTCT AAAAAAATCTTACCCGTA
katY_derep_rev	mutagenesis reverse primer to introduce the mutation TA31-32CT into YPK_3388 (*katY*) 5‘-UTR	pBO6886	TACGGGTAAGATTTTTTTAG ACATATATAAGTCCCCTT
katY_5‘-flank_fw	forward primer to amplify the upstream region (468 bp) of YPK_3388 (*katY)* for deletion of *katY*	pBO7212	TTTGTCGACTACGCCTTGTC CAATGTCAG
katY_5‘-flank rev	reverse primer to amplify the upstream region (468 bp) of YPK_3388 (*katY)* with an overlap to the downstream region (603 bp) of *katY* for deletion of *katY*	pBO7212	ATCCTCCCCTCTATTTAGAT ATAAGTCCCCTTTAAC
katY_3’flank_fw	forward primer to amplify the downstream region (603 bp) of YPK_3388 (*katY)* with an overlap to the upstream region (468 bp) for deletion of *katY*	pBO7212	GTTAAAGGGGACTTATATCT AAATAGAGGGGAGGAT
katY_3’flank_rev	reverse primer to amplify the upstream region (603 bp) of YPK_3388 (*katY)* for deletion of *katY*	pBO7212	TTTTCTAGATTCCTGAAATA TACCCGTCGC
katY_EP_fw	forward primer to check for deletion/complementation of YPK_3388 (*katY)*	-	CGGTAAGACAGGATTTCAGT AGGG
katY_EP_rev	reverse primer to check for deletion/complementation of YPK_3388 (*katY)*	-	GACTAGGCTTCGGTACTATT GGTG
katY_IP_fw	forward primer to check for deletion/complementation of YPK_3388 (*katY)*	-	CCTTACAGGCAATATCGCGC
katY_IP_rev	reverse primer to check for deletion/complementation of YPK_3388 (*katY)*	-	GGGTTGATTTACGTAAACCC T
pBAD-His_fw	forward primer to linearize the pBAD-His A plasmid for NEB Hifi Assembly	pBO7246	GGTACCATATGGGAATTCGA AG
pBAD-His_rev	reverse primer to linearize the pBAD-His A plasmid for NEB Hifi Assembly	pBO7246	GGTATGGAGAAACAGTAGA G

katY-His_fw	forward primer to amplify the 5'-UTR of YPK_3388 (*katY)* plus *katY* with a His-tag for complementation of Δ*katY*	pBO7246 pBO7251	TTTCCATGGGCCTTTTAGTT AAAGGGGACTT
katY-His_rev	reverse primer to amplify the 5'-UTR of YPK_3388 (*katY)* plus *katY* with a His-tag for complementation of Δ*katY*	pBO7246 pBO7251	TTTTTAGTGGTGATGGTGAT GATGGTTATTTTTTATATCA AAGCGATCA
katY_pBAD_fw	forward primer to amplify the 5'-UTR of YPK_3388 (*katY)* plus *katY* with a His-tag and an overlap to the pBAD-His plasmid for complementation of Δ*katY*	pBO7246	CTCTACTGTTTCTCCATACC GCCTTTTAGTTAAAGGGGAC
His__pBAD_rev	reverse primer to amplify the 5'-UTR of YPK_3388 (*katY)* plus *katY* with a His-tag and an overlap to the pBAD-His plasmid for complementation of Δ*katY*	pBO7246	TCGAATTCCCATATGGTACC TTAGTGGTGATGGTGATGAT G
pDM4_katY_Del _fw	forward primer to linearize the pDM4- *katY* -deletion plasmid for NEB Hifi Assembly	pBO7251	ATATAAGTCCCCTTTAACTA AAAGGC
pDM4_katY_Del _rev	reverse primer to linearize the pDM4-*katA*-deletion plasmid for NEB Hifi Assembly	pBO7251	CTAAATAGAGGGGAGGATT TATC
katY_pDM4_Del _fw	forward primer to amplify the 5'-UTR of YPK_3388 (*katY)* plus *katY* with a His-tag and an overlap to the pDM4- *katY* -deletion plasmid for complementation of Δ*katY*	pBO7251	AAATCCTCCCCTCTATTTAG TTAGTGGTGATGGTGATG
katY_pDM4_Del _rev	reverse primer to amplify the 5'-UTR of YPK_3388 (*katY)* plus *katY* with a His-tag and an overlap to the pDM4-*katY*-deletion plasmid for complementation of Δ*katY*	pBO7251	TAGTTAAAGGGGACTTATAT ATGTTAAAAAAAATCTTACC CG
trxAshort_ro_fw	forward primer to amplify YPK_4035 (*trxA*) short 5'-UTR with a T7 promoter for the construction of the runoff plasmid	pBO6857	AGAAATTAATACGACTCACT ATAGGGGAGATCAAAGAAT AACACCGT
trxAshort_ro_rev	reverse primer to amplify YPK_4035 (*trxA*) short 5'-UTR + 60 bp from ATG; reverse primer with EcoRV site for the construction of the runoff plasmid for structure probing and primer extension inhibition	pBO6857	GCCGGCATTATTATTATCGA CAACGGG

trxAshort_rep_fw	mutagenesis forward primer to introduce the mutation A24T into YPK_4035 (*trxA*) 5‘-UTR	pBO6858 pBO6859	CTACTGTTGGTTAATGCTAC TCCAACGAGGTAGACACAA TC
trxAshort_rep_rev	mutagenesis reverse primer to introduce the mutation A24T into YPK_4035 (*trxA*) 5‘-UTR	pBO6858 pBO6859	GATTGTGTCTACCTCGTTGG AGTAGCATTAACCAACAGTA G
trxAlong_rep_fw	mutagenesis forward primer to introduce the mutation A24T into YPK_4035 (*trxA*) 5‘-UTR	pBO6862	GCTACACCAACGAGGTAGA CCCAATCCTTTGGAGTAGAA CA
trxAlong_rep_rev	mutagenesis reverse primer to introduce the mutation A24T into YPK_4035 (*trxA*) 5‘-UTR	pBO6862	TGTTCTACTCCAAAGGATTG GGTCTACCTCGTTGGTGTAG C
RT_sodB_fw	forward primer for detection of YPK_1863 (*sodB)* by qRT-PCR	-	CTGCCGAAACGCTGGAATAC CATTATGG
RT_sodB_rev	reverse primer for detection of YPK_1863 (*sodB)* by qRT-PCR	-	GATCTCTTCCAGTGATTTGC CTGC
RT_sodC_fw	forward primer for detection of YPK_3445 (*sodC)* by qRT-PCR	-	GGGATTGGTGGTTAATGCAG ATGG
RT_sodC_rev	reverse primer for detection of YPK_3445 (*sodC)* by qRT-PCR	-	CACCGCCAGCATGGATCATT AAC
RT_katA_fw	forward primer for detection of YPK_2855 (*katA)* by qRT-PCR	-	GACACCGACTATTTCTCTCA ACCACG
RT_katA_rev	reverse primer for detection of YPK_2855 (*katA)* by qRT-PCR	-	GCTTCAGGAACTTGCGATAA CTCACC
RT_katY_fw	forward primer for detection of YPK_3388 (*katY)* by qRT-PCR	-	GGGCGAATAAACTGGAACT GACC
RT_katY_rev	reverse primer for detection of YPK_3388 (*katY)* by qRT-PCR	-	CGTATTCGTCAACACACCAG CCTTAG
RT_bgaB_fw	forward primer for detection of *bgaB* by qRT-PCR	-	GACTGCAACTACTCCAGCTT GGTTTG
RT_bgaB_rev	reverse primer for detection of *bgaB* by qRT-PCR	-	CTACTGCCAAACGAGAGAA TGACACC
RT_nuoB_fw	forward primer for detection of YPK_1561 (*nuoB)* by qRT-PCR	-	GATCCTCTCGAGCAACATG

RT_nuoB_rev	reverse primer for detection of YPK_1561 (*nuoB)* by qRT-PCR	-	TAAAGCAGGTTCCGGCCA
RT_gyrB_fw	forward primer for detection of YPK_0004 (*gyrB)* by qRT-PCR	-	TCGCCGTGAAGGTAAAGTTC
RT_gyrB_rev	reverse primer for detection of YPK_0004 (*gyrB)* by qRT-PCR	-	CGTAATGGAAGTGGTCTTCT

References

1. Nuss AM, Heroven AK, Waldmann B, Reinkensmeier J, Jarek M, Beckstette M, et al. Transcriptomic profiling of *Yersinia pseudotuberculosis* reveals reprogramming of the Crp regulon by temperature and uncovers Crp as a master regulator of small RNAs. PLOS Genetics. 2015;11: e1005087. doi:10.1371/journal.pgen.1005087

2. Bolin I, Norlander L, Wolf-Watz H. Temperature-inducible outer membrane protein of *Yersinia pseudotuberculosis* and *Yersinia enterocolitica* is associated with the virulence plasmid. Infection and Immunity. 1982;37: 506–512.

3. Hanahan D. Studies on transformation of *Escherichia coli* with plasmids. Journal of Molecular Biology. 1983;166: 557–580. doi:10.1016/S0022-2836(83)80284-8

4. Simon R, Priefer U, Pühler A. A broad host range mobilization system for *in vivo* genetic engineering: Transposon mutagenesis in Gram negative bacteria. Nat Biotechnol. 1983;1: 784–791. doi:10.1038/nbt1183-784

5. Yanisch-Perron C, Vieira J, Messing J. Improved Ml3 phage cloning vectors and host strains: Nucleotide sequences of the M13mp18 and pUC19 vectors. Gene. 1985;33: 103–119. doi:10.1016/0378-1119(85)90120-9

6. Milton DL, O'Toole R, Horstedt P, Wolf-Watz H. Flagellin A is essential for the virulence of *Vibrio anguillarum*. J Bacteriol. 1996;178: 1310–1319. doi:10.1128/jb.178.5.1310-1319.1996

7. Degrossoli A, Müller A, Xie K, Schneider JF, Bader V, Winklhofer KF, et al. Neutrophil-generated HOCl leads to non-specific thiol oxidation in phagocytized bacteria. Winterbourn C, editor. eLife. 2018;7: e32288. doi:10.7554/eLife.32288

8. Righetti F, Nuss AM, Twittenhoff C, Beele S, Urban K, Will S, et al. Temperature-responsive *in vitro* RNA structurome of *Yersinia pseudotuberculosis*. Proceedings of the National Academy of Sciences. 2016;113: 7237–7242. doi:10.1073/pnas.1523004113

9. Pienkoß S, Javadi S, Chaoprasid P, Nolte T, Twittenhoff C, Dersch P, et al. The gatekeeper of *Yersinia* type III secretion is under RNA thermometer control. PLOS Pathogens. 2021;17: e1009650. doi:10.1371/journal.ppat.1009650